NBSIR 79-1754

A Linearized Finite Difference Computation of Fluid Heating in an Enclosure

Ronald G. Rehm and Martin R. Cordes

Mathematical Analysis Division
Center for Applied Mathematics
National Engineering Laboratory

Howard R. Baum

Center for Fire Research
National Engineering Laboratory

John Lewis

Boeing Computer Services, Inc.
Mail Stop 9C-01
P.O. Box 24346
Seattle, Washington 98124

May 3, 1979

Interim Report

U.S. DEPARTMENT OF COMMERCE
NATIONAL BUREAU OF STANDARDS

NBSIR 79-1754

A LINEARIZED FINITE DIFFERENCE COMPUTATION OF FLUID HEATING IN AN ENCLOSURE

Ronald G. Rehm and Martin R. Cordes

Mathematical Analysis Division
Center for Applied Mathematics
National Engineering Laboratory

Howard R. Baum

Center for Fire Research
National Engineering Laboratory

John Lewis

Boeing Computer Services, Inc.
Mail Stop 9C-01
P.O. Box 24346
Seattle, Washington 98124

May 3, 1979

Interim Report

U.S. DEPARTMENT OF COMMERCE, Juanita M. Kreps, *Secretary*
Jordan J. Baruch, *Assistant Secretary for Science and Technology*
NATIONAL BUREAU OF STANDARDS, Ernest Ambler, *Director*

A Linearized Finite-Difference Computation of Fluid Heating in an Enclosure

Ronald G. Rehm[+]
Howard R. Baum[*]
John Lewis[++]
Martin R. Cordes[+]

[+] Center for Applied Mathematics, National Engineering Laboratory, National Bureau of Standards

[*] Center for Fire Research, National Engineering Laboratory, National Bureau of Standards

[++] Boeing Computer Services, Inc., Mail Stop 9C-01, P.O. Box 24346, Seattle, Washington 98124

Abstract

In an earlier paper, approximate equations of motion were derived which are applicable to nondissipative, very nonadiabatic, buoyant flows of a perfect gas. In the present paper, these approximate equations are recast in a form in which they can be integrated by finite difference techniques. These nonlinear equations are made dimensionless, specialized to two dimensions and linearized. Finite difference approximations, using central differences in space and leapfrog in time, are made to the linearized equations. To start the computation, a first-order scheme is used for the initial time step. The dependent variables are density, the horizontal and vertical velocity components and pressure, and these variables are defined at various positions within a grid cell (see Figure 1b). The computer time required for various size computations and the accuracies obtained are reported.

At each time step, a large sparse system of linear algebraic equations, the finite difference approximation to the elliptic equation for the pressure, must be solved. A hybrid method, combining the interative algorithm called conjugate gradients with a fast direct method for solving Poisson's equation, is used to solve the algebraic system efficiently and accurately. (Typically, the solution of the algebraic equations arising on a 31 x 31 mesh is determined to five significant figures after between two and five iterations of the conjugate gradients algorithm using from two to five seconds of CPU time on the N.B.S. UNIVAC 1108.)

Finally, results of some computations are presented using computer-generated plots. A discussion is given of the software required to generate these plots. A very brief discussion is presented of the analytical procedures required to obtain a solution to the differential equations describing heating of a homogeneous fluid. Computations of the solution to the difference equations are found to confirm the conclusions of the analysis. Also, these computations are found to yield flow fields which behave qualitatively the same as flow fields observed in a room fire. Examples of computations of the flow fields induced by heating in a stratified fluid are also presented and discussed.

Contents

I. Introduction

Convection in fluids heated from below has been of interest for over one hundred years. Much of this interest has arisen from astrophysical and geophysical research.[1-3] More recently, technological applications in areas such as nuclear reactor design, liquid natural gas transport, and fire safety have led to the analysis of phenomena occurring in very different ranges of geometrical and physical parameters than those considered in earlier studies.

The principal application of interest to the authors is buoyant convection induced in room fires. The National Bureau of Standards, acting through the Center for Fire Research, is involved in a wide rante of investigations into various physicaland chemical phenomena arising in unwanted fires. The buoyant convection studies reported here are part of that effort. The heavy mathematical and computational emphasis in this project, together with its intrinsic interest, have led to its sponsorship as a joint activity with the Center for Applied Mathematics. This report is meant to record the current status of the project. As such, it should be considered an interim working document, rather than an account of a completed piece of work.

The approximate equations governing the large scale motion of a gas in an enclosure driven by a prescribed volumetric heat source were derived in an earlier paper.[4] The resulting mathematical model, a "thermally expandable fluid," is rather different from other idealized fluid equations, such as the Boussinesq model, usually employed in buoyant convection studies. The differences arise from the need to consider large density variations in a closed geometry of limited vertical extent. This

combination of parameters also arises in some boiling water nuclear reactor studies, where a single fluid approach to the two phase flow results in a thermally expandable fluid model.[22,21]

Due to the complexity of the equations of interest and the limited experience in dealing with them, considerable care was necessary in developing numerical computation techniques. The thermally expanding fluid motions share some common features with both incompressible fluid flow and with the hydrodynamic models used in numerical weather prediction. A sampling of the techniques used in the analysis of these related equations may be found in references 5-9. A study of these methods led the authors to the conviction that the computational procedures should be developed on a related system of linear equations before nonlinear calculations were attempted.

Three features of the thermally expanding fluid model which were felt to be of particular importance are amenable to analysis within the context of a linear problem. They are the numerical computation of internal wave oscillations over many cycles, efficient calculation of the self adjoint elliptic equation governing the pressure distribution, and the use of a distributed, volumetric heat source of prescribed strength (as opposed to boundary conditions) to drive the motion in a rectangular enclosure. The linear system was chosen by formally linearizing the thermally expanding fluid model about a rest state stably stratified in the vertical direction. The linearized motion is driven by the prescribed heat source.

The homogeneous solutions to the problem posed above were studied by the authors in reference 10. These solutions are internal waves which arise due to the stable stratification. These waves were used to test

finite difference schemes for accuracy and stability. Second order accurate spatial differences were used in conjunction with both first and second order accurate time differencing to derive candidate finite difference approximations to the homogeneous (internal wave) equations. The finite difference equations were solved exactly by analytical means and compared with the known solutions to the continuous problem. The finite difference scheme used in the present study to solve the inhomogeneous equations was selected on the basis of the analysis reported in Reference 10.

This report describes the numerical implementation of the finite difference scheme selected on the basis of the analysis outlined above. The motions are driven by a prescribed distributed heat source located at the bottom of a rectangular enclosure. Section II presents the non-linear continuous equations derived in reference 4 and describes the linearization. The finite difference equations, incorporating second order central differences in space and leapfrog in time are shown in section III. The solution of the pressure equation, based on fast direct methods for solving Poissons equation[11] combined with an iterative conjugate gradient technique[12,13] is discussed in section IV. Section V outlines the solution procedure for the coupled set of linear finite difference equations. Several examples of computational results, together with the computer graphics used to display them, are described in Section VI. Finally, a summary of the work presented in this report is given in Section VII.

II. FORMULATION OF CONTINUOUS PROBLEM

A. Full Nonlinear Equations

In an earlier paper[4] nonlinear equations describing three dimensional thermally-driven buoyant flows in an enclosure had been derived and their properties discussed. In this section these nonlinear equations will be rewritten in a form appropriate for numerical integration by finite difference techniques. This recast set of equations is then linearized and the boundary conditions for the linear equations are presented.

As in Reference 4 we consider an inviscid, non-heat-conducting perfect gas. The magnitude and the spatial variation of the heat source (representing the exothermic reaction in a fire) are taken as known; justification for such a model is given in Reference 4. The fluid and the fire source are assumed confined in a closed rectangular room with the center of the source along the floor. In contrast to Reference 4, we consider only a completely enclosed room (no leaks), and we confine attention in the linear problem to the two dimensional evolution of the flow.

Equations (11) of Reference 4 are

$$\frac{\partial \rho}{\partial t} + \frac{\partial}{\partial x_i}(\rho u_i) = 0$$

$$\rho\left(\frac{\partial u_i}{\partial t} + u_j \frac{\partial u_i}{\partial x_j}\right) + \frac{\partial (p - p_0(t))}{\partial x_i} - \rho k_i g = 0 \qquad (1)$$

$$\rho c_p \left(\frac{\partial T}{\partial t} + u_j \frac{\partial T}{\partial x_j}\right) - \frac{dp_0}{dt} = Q(x_i, t)$$

$$p_0(t) = \rho R T$$

Here ρ is density, u_i the velocity in the $i^{\underline{th}}$ coordinate direction ($i = 1, 2, 3$), p is the pressure excess above the mean pressure $p_o(t)$ in the room, T the temperature, C_p the constant pressure specific heat, R the gas constant, g_i is the gravitational acceleration and $Q(x_i, t)$ the specified volumetric heat source. The spatially uniform mean pressure $p_o(t)$ depends only upon time and increases because of the heating within the room. It is determined in a completely enclosed room by the equation

$$\frac{dp_o}{dt} = \frac{\gamma - 1}{V} \int_V Q(x_i, t)\, dV \qquad (2)$$

where γ is the ratio of specific heats, V is the volume of the room and the integration is performed over this entire volume. Equation (2) is a thermodynamic statement that the mean pressure rise as a function of time is determined by the total heat added to the room. (Heat can only be added or removed volumetrically and not through the walls because thermal conduction and radiative transport have been ignored in this model.)

Equations (1), derived in Reference 4, are an approximate set of nonlinear equations which are applicable to highly nonadiabatic, nondissipative buoyant flows of a perfect gas in three dimensions. These equations were derived under the assumption that heat is added slowly compared with the time required to equilibrate the pressure over the spatial extent of the heat source, an assumption appropriate to flows induced by fires. They are characterized by the fact that the spatially uniform mean pressure appears in the energy and state equations while the spatially variable portion of the pressure appears only in the momentum equation. The equations admit buoyant or internal-wave

motions while "filtering out" high-frequency, acoustic waves. They reduce to the Boussinesq equations when heating is mild, total density variations are small, and variations in the mean background pressure can be neglected (as would be the case if the room considerated here were open or if the mean pressure variation were comparable to the spatial pressure perturbation.)

Equations (1), fully nonlinear and three-dimensional, will be recast into a form suitable for numerical computation. To do this, we take the substantial derivative of the equation of state and use this with the energy equation to eliminate the temperature. The resulting equation describes the evolution of the density under heating

$$\frac{\partial \rho}{\partial t} + u_i \frac{\partial \rho}{\partial x_i} = -\rho \frac{\partial u_i}{\partial x_i} = -\rho D(x_j,t) \qquad (3)$$

where

$$D(x_j,t) = \frac{1}{\gamma p_0(t)} \left[(\gamma-1) Q(x_j,t) - \frac{dp_0}{dt} \right] \qquad (4)$$

Equation (3) and the continuity equation identify $D(x_i, t)$ as the divergence

$$\frac{\partial u_i}{\partial x_i} = D(x_j,t) \qquad (5)$$

Finally, as in Reference 4, the equation for the spatially variable portion of the pressure is obtained by dividing the momentum equations by density and taking the divergence of these equations. The resulting equation is

$$\frac{\partial}{\partial x_i}\left(\frac{1}{\rho}\frac{\partial p}{\partial x_i}\right) = -\left[\frac{\partial}{\partial x_i}\left(u_j \frac{\partial u_i}{\partial x_j}\right) + \frac{\partial D(x_j,t)}{\partial t}\right] \qquad (6)$$

The boundary conditions on these equations are that velocity normal to any (impermeable) wall vanish.

$$u_i n_i = 0 \qquad (7)$$

where n_i are the normal components of a vector describing the boundary walls. From Eqs. (1) and these conditions, the appropriate boundary conditions on the pressure equation are obtained

$$k_i \frac{\partial p}{\partial n_i} = \rho g n_i k_i \tag{8}$$

The complete set of recast nonlinear equations are gathered and rewritten below

$$\begin{aligned}
&\frac{\partial \rho}{\partial t} + u_i \frac{\partial \rho}{\partial x_i} = -\rho D(x_j,t) \\
&\frac{\partial u_i}{\partial t} + u_j \frac{\partial u_i}{\partial x_j} = -\frac{1}{\rho}\frac{\partial p}{\partial x_i} + k_i g \\
&\frac{\partial}{\partial x_i}\left(\frac{1}{\rho}\frac{\partial p}{\partial x_i}\right) = -\left[\frac{\partial}{\partial x_i}\left(u_j \frac{\partial u_i}{\partial x_j}\right) + \frac{\partial D(x_j,t)}{\partial t}\right] \\
&\frac{dp_o}{dt} = \frac{\gamma - 1}{V}\int_V Q(x_i,t)\, dV \\
&D(x_i,t) = \frac{1}{\gamma p_o(t)}\left[(\gamma-1)Q(x_i,t) - \frac{dp_o}{dt}\right]
\end{aligned} \tag{9}$$

with boundary conditions

$$u_i n_i = 0 \quad , \quad k_i \frac{\partial p}{\partial n_i} = \rho g n_i k_i \tag{10}$$

B. Linear Equations

In this subsection the equations derived above are linearized and specialized to flow in two spatial dimensions ($x = x_1$, $y = x_2$) in a rectangular enclosure, $0 \le x \le L$, $0 \le y \le H$. The fluid in the enclosure initially is assumed to be arbitrarily stably stratified with density $\rho_o(y)$.

For convenience we will rewrite variables in terms of dimensionless quantities. This procedure can be applied to the three-dimensional, fully nonlinear equations also, but we will limit ourselves here to presenting only the equations in two dimensions in linearized form. Let u be the velocity in the horizontal or x-direction and v the velocity in the vertical or y-direction. Define the dimensionless variables, denoted by hats, as follows:

$$u = \sqrt{gH}\,\varepsilon\,\hat{u} \quad , \quad v = \sqrt{gH}\,\varepsilon\,\hat{v}$$
$$\rho = \rho_\infty [\hat{\rho}_0(\hat{y}) + \varepsilon\,\hat{\rho}]$$
$$p = p_\infty \hat{p}_0(\hat{t}) + \rho_\infty g H [\hat{P}_0(\hat{y}) + \varepsilon\,\hat{p}] \qquad (11)$$
$$x = H\hat{x} \quad , \quad y = H\hat{y}$$
$$t = (H/g)^{1/2}\,\hat{t}$$
$$Q = Q_0\,\hat{Q}(\hat{x},\hat{y},\hat{t})$$

where $\hat{p}_0(\hat{t}) = 1 + \varepsilon\,\hat{P}_1(t)$

and $$\varepsilon = (H/g)^{1/2}\,\frac{Q_0(\gamma-1)}{p_\infty} \qquad (12)$$

Here ρ_∞ is the ambient density and p_∞ the pressure at a specified altitude, here taken to be y=o. Q_0 is the magnitude of the volumetric heat source, and ε is a parameter relating the magnitude of the heat source to ambient pressure (or the energy per unit volume in the ambient gas).

For a heat source characteristic of the rate of heat release within a small room fire, the parameter ε is often small. Provided that the time does not become too large, then, so that the cumulative effects of the heat addition remain unimportant, ε can be used as a small parameter and Eqs. (10) can be formally linearized about the stably stratified rest state. The resulting two dimensional equations are

$$\frac{\partial\hat{\rho}}{\partial\hat{t}} + \hat{v}\,\frac{d\hat{\rho}_0}{d\hat{y}} = -\hat{\rho}_0(\hat{y})\,\hat{D}(\hat{x},\hat{y},\hat{t})$$
$$\frac{\partial\hat{u}}{\partial\hat{t}} = -\frac{1}{\hat{\rho}_0(\hat{y})}\,\frac{\partial\hat{p}}{\partial\hat{x}} \quad , \quad \frac{\partial\hat{v}}{\partial\hat{t}} = -\frac{1}{\hat{\rho}_0(\hat{y})}\left[\frac{\partial\hat{p}}{\partial\hat{y}} + \hat{\rho}\right] \qquad (13)$$
$$\frac{\partial}{\partial\hat{x}}\left(\frac{1}{\hat{\rho}_0(\hat{y})}\frac{\partial\hat{p}}{\partial\hat{x}}\right) + \frac{\partial}{\partial\hat{y}}\left(\frac{1}{\hat{\rho}_0(\hat{y})}\frac{\partial\hat{p}}{\partial\hat{y}}\right) = -\frac{\partial\hat{D}}{\partial\hat{t}} - \frac{\partial}{\partial\hat{y}}\left(\frac{\hat{\rho}}{\hat{\rho}_0(\hat{y})}\right)$$

$$\hat{D}(\hat{x},\hat{y},\hat{t}) = \frac{1}{\gamma}\left[\hat{Q}(\hat{x},\hat{y},\hat{t}) - AR\int_0^1 d\hat{y}\int_0^{1/AR} d\hat{x}\, Q(\hat{x},\hat{y},\hat{t})\right]$$

$$\frac{d\hat{P}_1(\hat{t})}{d\hat{t}} = AR\int_0^1 d\hat{y}\int_0^{1/AR} d\hat{x}\,\hat{Q}(\hat{x},\hat{y},\hat{t})$$

The aspect ratio AR of the room is the ratio of the height H to the length L of the rectangular room.

The boundary conditions corresponding to Eqs. (13) are that no mass flow from the enclosure:

$$\begin{aligned} \hat{u} &= 0 \qquad \text{at} \quad \hat{x} = 0 \quad \text{and} \quad \hat{x} = 1/AR, \\ \hat{v} &= 0 \qquad \text{at} \quad \hat{y} = 0 \quad \text{and} \quad \hat{y} = 1. \end{aligned} \tag{14}$$

These conditions, Eqs. (14), can be transformed into corresponding boundary conditions on the elliptic equation for the pressure, the fourth of Eqs. (13), using the two momentum equations in Eqs. (13):

$$\begin{aligned} \frac{\partial\hat{p}}{\partial\hat{x}} &= 0 \qquad \text{at} \quad \hat{x} = 0 \quad \text{and} \quad \hat{x} = 1/AR \\ \frac{\partial\hat{p}}{\partial n} &= \left(-\frac{\partial\hat{p}}{\partial\hat{y}}\right) = \hat{\rho} \qquad \text{at} \quad \hat{y} = 0 \\ \frac{\partial\hat{p}}{\partial n} &= \frac{\partial\hat{p}}{\partial\hat{y}} = -\hat{\rho} \qquad \text{at} \quad \hat{y} = 1 \end{aligned} \tag{15}$$

In the computations presented later, two forms for the ambient stratification have been selected. For most calculations an exponential stratification have been used:

$$\hat{\rho}_o(\hat{y}) = \exp\left(-\hat{y}/Y_s\right) \tag{16a}$$

This form includes the special case when Y_s is very large so that $\hat{\rho}_o(\hat{y})$ is practically constant. For some of the computations a "two layer" ambient stratification was used:

$$\begin{aligned} \hat{\rho}_o(\hat{y}) &= \exp\left(-\hat{y}/Y_s\right) \qquad \text{for } 0 \le \hat{y} \le Y_1 \\ \hat{\rho}_o(\hat{y}) &= \exp\left[-(\hat{y}-Y_1)/Y_{SUP} - Y_1/Y_s\right] \qquad \text{for } Y_1 \le \hat{y} \le 1 \end{aligned} \tag{16b}$$

The heat source was assumed to have a simple, separable form:

$$\hat{Q}(\hat{x},\hat{y},\hat{t}) = f(\hat{t})\left(\frac{\beta}{\pi}\right)^{1/2}\lambda \exp\left[-\beta(\hat{x}-\hat{x}_c)^2-\lambda\hat{y}\right] \qquad (17)$$

where $f(\hat{t}) = \tanh A\hat{t}$, A is a constant determining the rate at which the heat source is "turned on," and $\hat{x}_c$ is the location along the "floor" ($\hat{y}=0$) at which the center of the heat source is located. This form for the heat source $\hat{Q}$ was chosen as representative of a fire for analytical convenience only; another form could equally have been chosen.

Several important observations must be made about Eqs. (13)-(16). First, we note that $\hat{D}(\hat{x}, \hat{y}, \hat{t})$, from the form given in Eqs. (13), integrated over the rectangular region is zero. This fact, together with the boundary conditions (15), imply that the pressure equation the third of Eqs. (13), when integrated over the rectangular region is identically satisfied. Such a condition is necessary if the pressure equation is to have a solution at all since this elliptic equation has Neumann boundary conditions. When the pressure equation has a solution, this solution is only determined to within a constant, and the constant is determined to be consistent with the initial condition, or constant, chosen in the integration of the mean pressure equation, the last of Eqs. (13).

Second, it should be noted that the pressure equation in this linearized formulation is in fact separable: multiplication of the pressure equation by $\rho_0(y)$ shows that the coefficients of the derivatives of y in this equation are only functions of y (the coefficients of derivatives of x are unity). However, in the nonlinear formulation of this problem, the pressure equation is nonseparable. Since the linearized equations are being used to test solution techniques, the solution procedure for the pressure equation discussed in Section IV is for nonseparable elliptic equations.

III. FINITE DIFFERENCE EQUATIONS

In this section the finite difference equations used to approximate the linear partial differential equations, Eqs. (13), and the boundary conditions, Eqs. (14) and (15), will be presented and discussed. These difference equations are written on a "staggered mesh" in the style of reference 6 and were chosen to be approximations to the differential equations which are second-order accurate in both space and time.

In Figure 1a, the rectangular enclosure in dimensionless variables is shown together with a schematic representation of the spatial grids used for the finite difference scheme. The grid formed from solid lines represents the basic mesh into which the enclosure is divided: in general there are M mesh cells in the x-direction and N mesh cells in the y-direction. (The hat designation on dimensionless variables will now be dropped for convenience. Subsequently all quantities will be understood to be dimensionless.) Upon this basic mesh, the two components of the vector velocity (u, v) and single component of the vector vorticity $\omega = \frac{\partial v}{\partial x} - \frac{\partial u}{\partial y}$ are defined.

The second grid, formed by joining the center points of the basic grid cells and denoted by dashed lines, is that upon which scalar quantities such as density ρ and pressure p are defined. In Figure 1a the densities in the left-hand column of cells and in the bottom row of cells are shown to indicate how they are enumerated for the numerical computation.

In Figure 1b a typical mesh cell is shown, illustrating where all of the dependent variables in the finite difference scheme are defined relative to the cell.

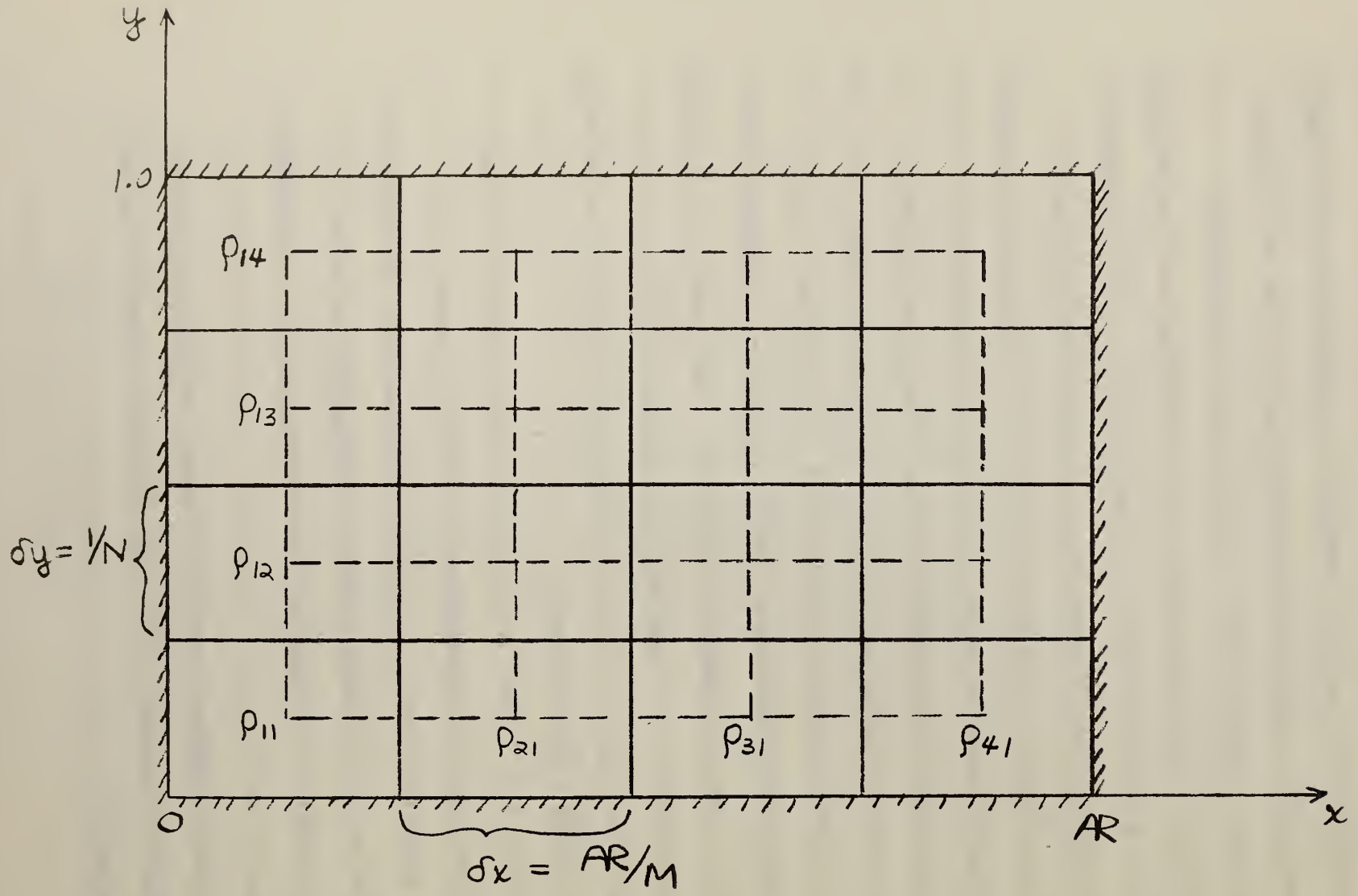

Fig. 1a Rectangular enclosure in dimensionless variables $0 \leq x \leq AR$, $0 \leq y \leq 1$. The mesh upon which the difference scheme is based is shown schematically for ($M = N = 4$) as a grid of solid lines. The mesh of dashed lines joins the center points of the basic mesh cells and is the grid upon which the pressure computation is performed.

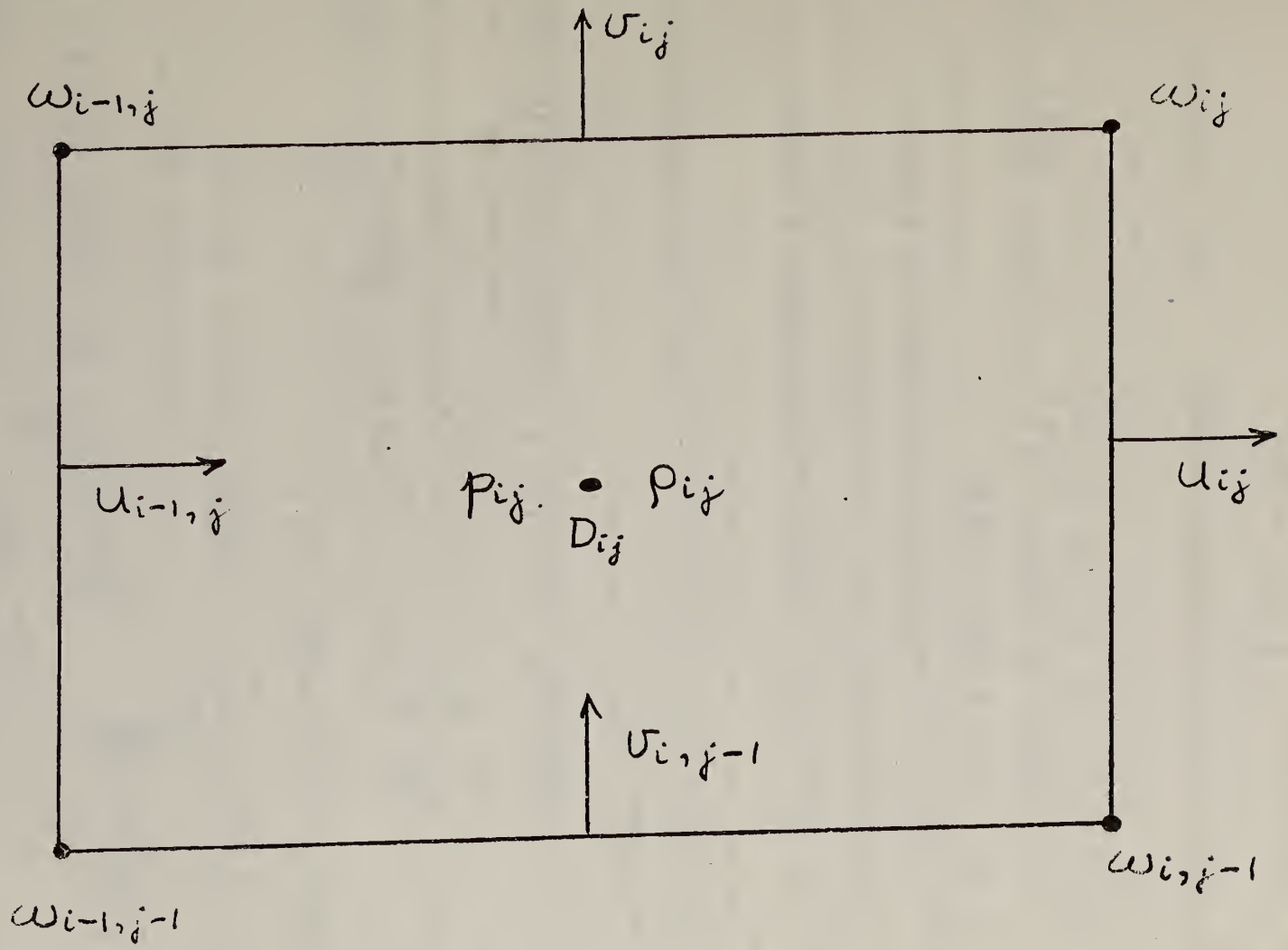

Fig. 1b A typical mesh cell, with center located at x = (i - 1/2) δx and y = (j - 1/2) δy, illustrating where all dependent variables for the finite difference scheme are defined.

The following discretely evaluated functions will denote approximations to the corresponding analytical solutions to Eqs. (13):

$$u_{ij}^{n} \cong u(i\delta x, (j-\tfrac{1}{2})\delta y, n\delta t)$$
$$v_{ij}^{n} \cong v((i-\tfrac{1}{2})\delta x, j\delta y, n\delta t)$$
$$\rho_{ij}^{n} \cong \rho((i-\tfrac{1}{2})\delta x, (j-\tfrac{1}{2})\delta y, n\delta t) \qquad (18)$$

$$p_{ij}^{n} \cong p((i-\tfrac{1}{2})\delta x, (j-\tfrac{1}{2})\delta y, n\delta t)$$
$$D_{ij}^{n} = D((i-\tfrac{1}{2})\delta x, (j-\tfrac{1}{2})\delta y, n\delta t), \quad \rho_{0,j} = \rho_0((j-\tfrac{1}{2})\delta y)$$
$$\omega_{ij}^{n} \cong \omega(i\delta x, j\delta y, n\delta t)$$

where $\delta x = AR/M$ and $\delta y = 1/N$ are the mesh cell sizes in the x- and y-directions respectively and where δt is the time-step size. Such a staggered grid is commonly used for multidimensional finite difference integrations.[6]

With this notation, the following set of finite difference equations was used to approximate Eqs. (13):

$$\rho_{ij}^{n+1} - \rho_{ij}^{n-1} = -\frac{2\delta t}{4\delta y}(v_{ij}^{n} + v_{i,j-1}^{n})(\rho_{0,j+1} - \rho_{0,j-1}) - \rho_{0,j} D_{ij}^{n} 2\delta t \qquad (19a)$$

$$u_{ij}^{n+1} - u_{ij}^{n-1} = -\frac{2\delta t}{\delta x}\frac{1}{\rho_{0,j}}(p_{i+1,j}^{n} - p_{ij}^{n}) \qquad (19b)$$

$$v_{ij}^{n+1} - v_{ij}^{n-1} = -\frac{2\delta t}{\delta y}\frac{2}{\rho_{0,j+1}+\rho_{0,j}}\left[(p_{i,j+1}^{n} - p_{ij}^{n}) + \frac{\delta y}{2}(\rho_{i,j+1}^{n} + \rho_{ij}^{n})\right] \qquad (19c)$$

$$\frac{1}{\delta x^2}\left[\frac{1}{\rho_{0,j}}(p_{i+1,j}^{n} - 2p_{ij}^{n} + p_{i-1,j}^{n})\right]$$
$$+ \frac{1}{\delta y^2}\left[\frac{2(p_{i,j+1}^{n} - p_{ij}^{n})}{\rho_{0,j+1}+\rho_{0,j}} - \frac{2(p_{ij}^{n} - p_{i,j-1}^{n})}{\rho_{0,j}+\rho_{0,j-1}}\right]$$
$$= -\frac{1}{\delta y}\left[\frac{\rho_{i,j+1}^{n} + \rho_{ij}^{n}}{\rho_{0,j+1}+\rho_{0,j}} - \frac{\rho_{ij}^{n} + \rho_{i,j-1}^{n}}{\rho_{0,j}+\rho_{0,j-1}}\right] - \frac{D_{ij}^{n+1} - D_{ij}^{n-1}}{2\delta t} \qquad (19d)$$

$$p_1^{n+1} - p_1^{n-1} = 2\delta t\, K f^{n} \qquad (19e)$$

where $D_{ij}^{n} = \frac{1}{\delta}(Q_{ij} - K)f^{n}$

$$Q_{ij} = \left(\frac{\beta}{\pi}\right)^{1/2} \lambda \exp\left[-\beta((i-\tfrac{1}{2})\delta x - x_c)^2 - \lambda(j-\tfrac{1}{2})\delta y\right]$$

$$K = \frac{1}{MN} \sum_{i=1}^{M} \sum_{j=1}^{N} Q_{ij} \qquad (20)$$

$$f^n = \tanh(A n \delta t)$$

Spatial derivatives in Eqs. (13) are approximated by central differences and leapfrog is used for time derivatives. These equations have second order truncation errors in both space and time; i.e., the local discretization errors made in approximating the differential equations (13) by these difference equations is $0(\delta x^2)$, $0(\delta y^2)$, $0(\delta t^2)$. In the first three of Eqs. (19), the time derivatives have been replaced by central differences which give explicit formulae for computing dependent variables at a new time level, a difference method commonly referred to as the leapfrog method. With this method dependent variables at two previous time levels are required to compute the quantities at a new time level; hence the scheme is said to be a three-time-level scheme. A starting procedure is required to generate the dependent variables at the first time level, given these quantities initially (at t=0).

To obtain dependent variables at the first time level, an explicit first-order (in time) procedure is used:

$$\rho'_{ij} - \rho^\circ_{ij} = -\frac{\delta t}{4\delta y}(v^\circ_{ij} + v^\circ_{i,j-1})(\rho_{o,j+1} - \rho_{o,j-1}) - \rho_{o,j} D^\circ_{ij} \delta t \qquad (21a)$$

$$u'_{ij} - u^\circ_{ij} = -\frac{\delta t}{\delta x} \frac{1}{\rho_{o,j}} (p^\circ_{i+1,j} - p^\circ_{ij}) \qquad (21b)$$

$$v'_{ij} - v^\circ_{ij} = -\frac{\delta t}{\delta y} \frac{2}{\rho_{o,j+1} + \rho_{o,j}} \left[(p^\circ_{i,j+1} - p^\circ_{ij}) + \frac{\delta y}{2\vartheta}(\rho'_{i,j+1} + \rho'_{ij})\right] \qquad (21c)$$

$$\frac{1}{\rho_{o,j}}(p^\circ_{i+1,j} - 2p^\circ_{ij} + p^\circ_{i-1,j}) + \frac{1}{\delta y^2}\left[\frac{2(p^\circ_{i,j+1} - p^\circ_{ij})}{\rho_{o,j+1} + \rho_{o,j}} - \frac{2(p^\circ_{ij} - p^\circ_{i,j-1})}{\rho_{o,j} + \rho_{o,j-1}}\right]$$
$$= -\frac{1}{\delta y}\left[\frac{\rho'_{i,j+1} + \rho'_{ij}}{\rho_{o,j+1} + \rho_{o,j}} - \frac{\rho'_{ij} + \rho'_{i,j-1}}{\rho_{o,j} + \rho_{o,j-1}}\right] - \frac{D'_{ij} - D^\circ_{ij}}{\delta t} \qquad (21d)$$

$$p'_1 - p^\circ_1 = \delta t K f^\circ \qquad (21e)$$

where all supplementary quantities are defined in Eqs. (20).

The computational procedure by which Eqs. (19) and (21) are solved is very important. At first inspection, it may appear that Eqs. (21) are implicit for example. However, when Eq. (21a) is solved first for density, Eq. (21d) second for pressure and the remaining equations are solved subsequently, Eqs. (21) are found to be explicit. Also, the time level associated with the discretely evaluated variable representing pressure may not be the expected one. These considerations are discussed in Section V.

The two forms for the ambient density stratification, given by Eqs. (16a) and (16b) in the continuous case, have been used in discretized form in all of the computations presented in Section VI. For most computations n exponential stratification was used

$$\rho_{o,j} = \exp\left[-(j-\tfrac{1}{2})\,\delta y / Y_s\right] \qquad (22a)$$

We note that, when Y_s is taken to be large (generally 10^6 in our computations), the ambient density is essentially constant. For some computations, a discretized "two-layer" model of the ambient stratification was used:

$$\rho_{o,j} = \exp\left[-(j-\tfrac{1}{2})\,\delta y / Y_s\right] \quad \text{for } 1 \le j \le J_s \qquad (22b)$$

$$\rho_{o,j} = \exp\left[-(j-J_s)\,\delta y / Y_{sup} - (J_s-\tfrac{1}{2})\,\delta y / Y_s\right] \quad \text{for } J_s \le j \le N \qquad (22c)$$

In all cases, the initial velocities u^o_{ij}, v^o_{ij} and the density deviation from ambient ρ^o_{ij} were taken to be zero.

Boundary conditions for these difference equations are obtained from Eqs. (14) and (15): they are

$$\begin{aligned} u^n_{0,j} &= u^n_{M,j} = 0 \quad &&\text{for } 1 \le j \le N \\ v^n_{i,0} &= v^n_{i,N} = 0 \quad &&\text{for } 1 \le i \le M \end{aligned} \qquad (23a)$$

and

$$\left.\begin{aligned} \tilde{p}^{n}_{0,j} - \tilde{p}^{n}_{1,j} &= 0 \\ \tilde{p}^{n}_{M+1,j} - \tilde{p}^{n}_{M,j} &= 0 \end{aligned}\right\} \quad \text{for } 1 \le j \le N$$

$$\left.\begin{aligned} \tilde{p}^{n}_{i,0} - \tilde{p}^{n}_{i,1} &= \delta y/2\,(\tilde{\rho}^{n}_{i,0} + \tilde{\rho}^{n}_{i,1}) \\ \tilde{p}^{n}_{i,N+1} - \tilde{p}^{n}_{i,N} &= -\delta y/2\,(\tilde{\rho}^{n}_{i,N+1} + \tilde{\rho}^{n}_{i,N}) \end{aligned}\right\} \quad \text{for } 1 \le i \le M \qquad (23\text{A})$$

The pressures and densities denoted by a tilde are values defined beyond the grid defined in Figure 1. These values can be regarded therefore as quantities defined in fictitious cells surrounding the rectangular region of interest. However, in the procedure for solving the linear algebraic system of equations for the pressure, the boundary conditions are incorporated directly into the system: the pressure and density values in the fictitious cells cancel and never appear in the final system of equations for the pressure in the rectangular region.

The procedure used to solve the discretized pressure equation is discussed in Section IV. Before this discussion, however, we note that the discrete pressure equation together with its boundary condition retains the important property of the partial differential equation for the pressure with its boundary conditions noted at the end of Section II. The definition of D^{n}_{ij} presented in Eqs. (20) shows that

$$\sum_{i=1}^{M} \sum_{j=1}^{N} D^{n}_{ij} = 0 \qquad (24)$$

This fact, plus that concerning the boundary conditions noted above, allows one to demonstrate that, for the discretized pressure equation, the left hand side and the right hand side, when summed over all grid points, each vanish identically. This important condition must hold for a solution to exist to the linear algebraic system for the discretized pressure field; it is discussed further in the next section (see Eqs. (29) and (30)).

IV. THE SOLUTION OF THE PRESSURE EQUATION

At each time step in the fully nonlinear problem it is necessary to calculate the solution to the non-separable elliptic equation

$$\frac{\partial}{\partial x_i}\left(\frac{1}{\rho(x,y)}\frac{\partial}{\partial x_i}P(x,y)\right) = f(x,y) \qquad (25a)$$

on the rectangle R, subject to the Neumann boundary conditions

$$k_i \cdot \frac{\partial P}{\partial x_i}(x,y) = \rho(x,y)\, g(x,y) n_i k_i \text{ on } \partial R \qquad (25b)$$

Here, the density ρ, the forcing function f, and the boundary function g all depend on time, but are known to us. (In the linear computation reported here, $\rho(x, y)$ is replaced by $\rho_o(y)$, which yields a separable elliptic equation as noted in Section II. However, the solution procedure is developed for the fully nonlinear problem.) In the discretization, Equations (25) are replaced by finite difference equations, Eqs. (19d) or (21d) and (23) in Section 3. The finite difference equations (19d) or (21d) then directly incorporate the boundary conditions (23). Hence, the calculation of the pressure requires only the solution of the linear equations represented by these combined equations.

Physically Equations (25) produce a unique solution only when the pressure is prescribed at some particular point. Equivalently, there is a unique solution with mean pressure zero. Given any particular solution, we can generate a new solution by adding an arbitrary constant to the pressure. The linear equations (19d), (21d) behave analogously; the linear system has a family of solutions such that there is a unique solution with mean pressure zero, and the family of solutions can be generated by adding constants to any particular solution.

The calculation of the pressure requires us to successfully meet the constraints of the larger system of equations:

the solution method must take into account non-uniqueness; the solution method must be able to solve large linear systems accurately, since there are NM equations (19d); and it is very important that the s lution be obtained quickly since the calculation is made at each time step.

The finite difference equations (19d) can be conveniently represented in matrix notation as

$$Ap = z \tag{26}$$

where $p = (p_{11}, P_{12}, P_{13}, \cdots P_{1M}, P_{21}, P_{22}, \cdots P_{2M}, \cdots P_{N1}, \cdots P_{NM})^T$ is a vector of dimension NM, as it z, the vector of right sides from Eqs. (19d) or (21d) (modified by boundary conditions (23)). The matrix A gives the coefficients from the density and the finite differences. Here the subscript T denotes transpose. Although A is of dimension NM by NM, it has at most 5 non-zero elements in any row.

As noted above, the solution to Eqs. (25) is determined only to within an additive constant. Similarly, the solution to the system of linear equations (26) is also determined only to within an additive constant. The non-uniqueness of the solution is represented by

$$A(p + \alpha e) = z \tag{27}$$

where $e = (1, 1, 1, 1 \ldots 1)^T$; α is any scalar and p any solution of (26). This can be represented also as:

$$Ae = 0. \tag{28}$$

which is the statement that e is an eigenvector of A corresponding to zero eigenvalue. The solution $\bar{p}$ with mean pressure zero is the solution of (26) which satisfies

$$\bar{p}^T e = 0. \tag{29}$$

The existence of a solution requires the following equation to hold

$$z^T e = 0. \tag{30}$$

This condition on the difference equations (19d) or (21d), incorperating boundary conditions (23b), is simply the statement that the right hand sides sum to zero. As noted at the end of the last section, see particularly Eq. (24) and the surrounding discussion, this condition is guaranteed by the formulation of the linearized difference equations. It also must be guaranteed when the nonlinear difference equations are developed. We assume equation (30) and proceed to calculate the solution to the linear system (26) which satisfies the mean pressure requirement (29).

Standard direct factorization methods (Gaussian elimination) for calculating the solution to (26) are infeasible, because 0 $((NM)^2 M)$ operations at best are necessary. Iterative methods are often used to solve sparse linear systems: the method of successive over-relaxation (SOR) is probably best known. However, a successful implementation of SOR requires at least a good estimate of the over-relaxation parameter. The convergence rate even with an optimal parameter still yields 0 ((NM)N log N) operations for a solution of (26).[22]

The specific structure of the finite difference operation on the rectangle R makes possible special fast direct methods for the solution of separable elliptic equations. The algorithms discussed in Schwartztrauber and Sweet[11] are the most current extensions of the ideas behind the fast finite Fourier transform. However, even these general algorithms require separability (the coefficients of the derivatives with respect to x involve only x; the coefficients of the derivatives with respect to y are functions only of y), and the solution procedure which will be presented here is for the case of interest in nonlinear problem. The pressure equation can be transformed to separable form only if ρ is known analytically and has two continuous derivatives.[12] Since ρ is known only on the staggered grid, these conditions are not met.

The solution method we have adopted is a hybrid method which combines an iteractive algorithm, conjugate gradients (denoted c.g.), with a fast direct Poisson solver. The conjugate gradients algorithm provides an iterative technique for solving Ap = z, provided A is a positive definite symmetric matrix (equivalently, all eigenvalues of A are positive). Each iteration of conjugate gradients requires one matrix-vector product, A times x or roughly 5 MN operations. However, the convergence rate depends critically on the ratio, $\kappa = \lambda_{NM}/\lambda_1$, the largest eigenvalue divided by the smallest. The ratio is large for the linear system (26), and convergence is fast only if κ is close to unity. To improve (drastically) the rate of convergence, we write, following Concus and Golub,[12]

$$A = A_s + A_n \tag{31}$$

where A_s and A_n are matrices chosen so that $A_s^{-1}z$ can be calculated quickly with a fast Poisson solver and the entries in A_n are small compared to A_s.

The best choice of A_s is not known theoretically. Our solution is to take

$$A_s = D\ LD \tag{34}$$

where L is the finite difference matrix using a five-point difference formula for the Poisson equation $\nabla^2 P = f$ with Newmann boundary conditions. Here D is a positive diagonal matrix chosen so that diagonal (A_s) = diagonal (A). The remainder A_n is a matrix with zero main-diagonal, and non-zero entries present on only four off-diagonals. Such a choice is justified on empirical grounds only if the conjugate gradient convergence rate is sufficiently fast. For our test problems this has certainly been the case. There is also some theoretical basis for this choice; see Concus & Golub[12].

Then we formally replace the equation

$$Ap = z$$

by

$$(D\ AD)\ a = Dz \tag{32}$$

where DAD is a new "scaled" matrix and Dz is the corresponding scaled right hand side. We then solve the scaled problem using conjugate gradients. The solution p of (26) is then Da.

If we have made a suitable choice for A_s, the eigenvalue ratio λ_{MN}/λ_1 for the matrix D AD will be very close to the optimum value, unity. The solution of (32) requires one matrix-vector product Ax, and the solution of

$$A_s x = y \tag{33}$$

at each iteration. (The matrix D does not appear explicitly in the actual algorithm.) The details of this general approach are given in Concus, Golub and O'Leary.[13] Although the solution of (33) requires 0 (NM log N) operations, the entire process will be efficient if we need to solve (33) only a very few times. Typical calculations for our code require no more than three to five Poisson solutions to obtain the solution of (26).

The only difficulty with the approach outlined above is the non-uniqueness of the solution. The matrix A which represents the finite difference equations is only positive-semidefinite, since $\underset{\sim}{e}$ is an eigenvector corresponding to the eigenvalue 0. However, all other eigenvalues are positive. The iterations in the conjugate gradients algorithm will generate a solution orthogonal to $\underset{\sim}{e}$ if and only if the iterations are begun with a vector orthogonal to $\underset{\sim}{e}$.

The natural solution produced by the method is the zero mean pressure solution; any other solution can be produced from this particular solution by adding a constant.

There is an additional complication in the hybrid algorithm since both A and L, the discrete Poisson operator, are singular; Ae = Le = $\underset{\sim}{0}$. The iteration matrix D AD has a single zero eigenvalue with eigenvector $D^{-1}e$. In [14] we show that for a more general splitting of matrix A,

the iteration matrix corresponding to D AD has the desired single zero eigenvalue with both A and the matrix corresponding to D singular if and only if the corresponding eigenvectors of A and the more general D are not orthogonal. This can be assumed in our calculation since $e^T D^{-1} e = \frac{1}{d_{11}} + \frac{1}{d_{12}} + \ldots + \frac{1}{d_{NM}}$ and all the d_{ii} are positive.

It is shown in [14] that a choice of A_s with the same eigenvector of zero eigenvalue as A is optimal in some respects, but such a choice seems difficult to realize. Our simpler choice, as outlined above, proves entirely satisfactory. However, we must note that the search direction in the c.g. iteration must now be orthogonal to $D^{-1}e$, not e. This requires that the solution to the discrete Poisson equation Lx = y be normalized to mean pressure zero. This normalization must be done by the user of the Schwarztrauber-Sweet routines,[11] and probably is also necessary for other fast Poisson solvers.

V. Computational Procedure for Solving Linear Finite Difference Equations

In Section III the finite difference equations describing linearized heating, Eqs. (19)-(23), were presented, and in Section IV the procedure used to solve the pressure equation was described. In this section the solution procedure for the complete set of linearized difference equations will be presented and some aspects of the computation will be discussed.

Since the finite difference scheme, Eqs. (19) is a three level scheme. values of velocities and density at two levels of time are required to initiate the computation. Equations (21), a scheme first order in time, were introduced to provide values of the dependent variables u^1_{ij}, v^1_{ij} and ρ^1_{ij} given initial data. Equations (21) are solved in the following order. First the densities ρ^1_{ij} are obtained from Eq. (21a). Then the pressures p^0_{ij} are obtained, using the ρ^1_{ij}, from Eq. (21d). Finally the velocities u^1_{ij}, v^1_{ij} are computed from (21b) and (21c).

One point in this process is noteworthy. The initial pressure data provided to the computational scheme is used only as an initial "guess" for the iterative pressure-solving procedure: the initial values of the pressure p^0_{ij} are obtained using ρ^1_{ij}. Such a procedure was adopted because our analytical studies of the finite difference scheme first order in time demonstrated that it was most appropriate for reproducing the test problem (see Reference 10 for details).

In subsequent time steps the order in which the difference equations are solved is changed somewhat. First, the pressure equations, Eq. (19e) for the mean pressure and Eq. (19d) for the pressure variation, are solved. Then the density and the two velocities are updated using Eqs. (19a)-(19c).

It should be noted that in both the first time step and subsequent ones, the solution to the pressure equation assures that the velocity components will satisfy the proper divergence condition. Equation (5) is the imposed condition on the divergence of the velocity in the continuous case; this equation also applies in the linear problem, with the dimensionless $D(x,y,t)$ being specified by the fourth of Eqs. (9). The discrete version of Eq. (5) is

$$\frac{1}{\delta x}\left(u_{i,j}^{n+1} - u_{i-1,j}^{n+1}\right) + \frac{1}{\delta y}\left(v_{ij}^{n+1} - v_{i,j-1}^{n+1}\right) = D_{ij}^{n+1} \tag{35}$$

where D_{ij}^{n} is given by Eqs. (20). This condition is very important since it specifies, in the discrete (and linear) case, what effect the heat source imposes through continuity upon the velocity field. Substituting for u_{ij}^{n+1}, v_{ij}^{n+1} from Eqs. (19b) and (19c), and using Eq. (35) again, with $n-1$ replacing $n+1$, yields the equation for the pressure, Eq. (25d) for all steps after the first. Hence proper solution of this pressure equation assures that the velocities at time step $n+1$ will satify the proper divergence condition, Eq. (35). An analogous argument for the first time step, using Eq. (21b), (21) and (35), shows that the pressure equation (21d) assures the proper divergence condition at the first time step.

When there is no imposed heating, so that $Q_{ij}^{n} = D_{ij}^{n} = 0$, Eqs. (19) and (21) are homogeneous (as noted earlier). In Reference 10 the homogeneous equations (19) with the first-order starting procedure implied by the homogeneous form of Eqs. (21) were solved analytically for internal waves in a rectangular enclosure. Comparisons were made between this analytical solution to the finite difference equations and one generated by computational

procedures. These comparisons showed that the accuracy with which the difference equations were solved computationally was determined by the accuracy specified for the solution of the pressure equations (19d) (or (21d) on the first time step). When the accuracy specified for the pressure equation was 10^{-5}, the analytically and computationally generated solutions agreed to 1 or 2 parts in 10^{5}.

Further comparisons were made between the analytical solution to the finite difference equations and the analytical solution to the continuous problem, the homogeneous form of Eqs. (13). These solutions differ by the truncation error resulting from replacing differential equations by difference equations. The truncation errors in turn depend upon the spatial grid size relative to characteristic spatial variations in the solution and upon the time step size relative to characteristic temporal variations in the solution. Internal waves in a rectangular enclosure were examined analytically to test the finite difference schemes and computational procedure. Such waves are expected once the fire has stratified the gas in the room.

A single internal-wave mode was specified initially (in either continuous or discretized form) and its time history was calculated by way of the differential or difference equations. The mode was specified by two integers, the number of half wave lengths in the x-direction and the number of half wavelengths in the y-direction filling the rectangular enclosure and satisfying boundary conditions. Specification of the mode then determined the eigenfrequency, through the equations of motion, with which this characteristic mode oscillated. The stability of the finite difference equations was found to require that

$$\frac{\delta t^2}{4Y_s} \frac{\sinh(\delta y/Y_s)}{\delta y/Y_s} \leq 1$$

This condition requires that the time step size be a fraction of the Brunt-Vaisala period for the ambient fluid, eigenfrequencies being inversely proportional to this period. Accuracy of the finite difference equations was found to require that the mode number relative to the mesh-cell number M in the x-direction be small, the mode number relative to the mesh-cell number N in the y-direction be small and the time step size relative to the Brunt-Vaisala period be small.

As an example, a 5 by 2 mode internal wave was calculated for an ambient stratification parameter Y_s (see equation 16a) equal to unity. For this stratification, the Brunt-Vaisala period is 2π in dimensionless time units. A 31 x 30 mesh was employed, with $\delta t = 0.25$. At a dimensionless time t=10, the discrete and continuous solutions differed by about 3%. During this time the discrete solution oscillated about the continuous result in an irregular fashion. This behavior in the discretization error is characteristic of the spurious computational mode introduced by the leapfrog time differencing procedure. The continuous eigenvalue σ which determines the actual period of the mode under consideration is $\sigma=.92807$ for this example. The corresponding discrete mode eigenvalue σ^* for this problem may be analytically calculated[10] to be $\sigma^*=.923955$. Thus, the computational scheme should be able to follow oscillations sufficiently accurately to avoid errors due to phase shifts between modes for times t $0(100)$. Throughout the time interval $0 \leq t \leq 10$, the finite difference equations were solved computationally to a few parts in 10^5. This estimate is based on direct comparison between the analytically obtained and numerically computed results.

Last, we mention briefly computational times required. All computations reported in the next section (and those performed for results reported in Reference 2) were carried out on the N.B.S. UNIVAC 1108. Most computations were performed using M = 31 and N = 31 for the mesh and were run for up to two hundred time steps. For a calculation performed starting with a stratified fluid, between three and four iterations on average were taken by the conjugate gradients portion of the pressure solver and the computer time required per time step was between 4 and 5 seconds. For example, one computation of 70 time steps took 302 seconds of CPU time and another took 316 seconds. For a calculation in an essentially unstratified fluid (in which the elliptic equation for the pressure becomes Poisson's equation), only one iteration was required and about 2 seconds per time step was taken. In this case, a computation run for 200 time steps required 402 seconds of CPU time.

Computations on smaller meshes required substantially less time. For example, a computation performed for a stratified fluid using M = 7 and N = 8 required 66 seconds of CPU time to run 200 time steps. Another calculation, performed for an unstratified fluid with M = 15 and N = 16 and also run for 200 time steps required 122 seconds.

The computational times quoted do not include CPU time required to produce the computer-generated plots discussed in the next section. When plots were generated, the results were read to file during the computation and processed later to produce the graphics. Computer time required for the graphics will be discussed in the next section.

VI. Computer-Generated Results

Because Egs. (13) with boundary conditions (14) and (15) are linear, they can be solved analytically (and these expressions evaluated numerically) or by a combination of analytical and computational techniques. Unfortunately, neither of these procedures has been implemented as a computer code at this time so that comparison of the results reported in this section with results obtained by an alternate procedure cannot be made yet. Presently, we are implementing one approach using a mixture of analytical and numerical techniques, and we will make such comparisons later.

A. Graphics

From the finite difference equations (19), we see density, horizontal and vertical velocity components and pressure are all computed dependent variables at each time step. Typically in the computations we have run, we have used a grid composed of 31 x 31 mesh boxes: hence at each time we have 4 dependent variables, each being calculated at approximetely 1000 points. Clearly with such a large number of values computed, graphical display is required to digest the results. Generally we have used two computer plotting routines to allow us to visualize results; both routines were developed by the Mathematical Analysis Division specifically for this application and have been found to be essential for rapid assimilation of results. Most plots shown in this report are direct reproductions of these computer-generated plots.

Both plotting routines display the dependent variables on the rectangular region of computation. One routine displays profiles of the horizontal and vertical velocity components. The other plotting routine displays contours

of constant density (isopycnic contours).

The horizontal velocity is plotted as a function of vertical position at prescribed horizontal locations, together with plots of vertical velocity as a function of horizontal position at prescribed vertical locations. (The locations at which horizontal or vertical velocity plots are desired can be specified.) These superimposed plots give a clear picture of the velocity field at any instant of time.

At a horizontal location, this plotting routine takes the values of the computed horizontal velocity components at the vertical mesh points and fits this data with cubic splines using a package "splines under tension" written by A.K. Cline.[15,16] Since the vertical mesh points at which the horizontal velocity components are computed is staggered with respect to the grid lines covering the computational region, horizontal velocities are not computed at the top or at the bottom boundaries. The last computed horizontal velocity is one half mesh point from the boundary, and the velocity profiles are extrapolated to the boundaries using the fitted cubic splines (not under tension).

Similarly at the vertical location, the plotting routine fits the computed vertical velocity values as a function of horizontal position with cubic splines. However, for the vertical velocity, the normal derivative at the left and right walls can be shown to be zero for the linearized equations.

Using this condition and the values of the vertical velocity at the two points adjacent to each wall, a quadratic equation was used to extrapolate the value of the vertical velocity at each wall. Then the package

written by A.K. Cline was used to fit the vertical velocity data and the end point information by cubic splines (not under tension). An earlier version of this package is described in references 15 and 16.

Finally, the velocity plots shown below were prepared with an interactive Fortran program using Tektronix Plot 10 Advanced Graphing II software and Terminal Control System (TCS) software.[17,18] The display device is a Tektronix 4014 display terminal.

The second plotting routine gives constant-density contours. It first creates an intermediate code with an interactive Fortran using the NCAR graphics software CONREC and DASHCHAR[19] together with the system plot package and the Tektronix Plot 10 TCS. Then the intermediate form is translated using the NCAR portable graphics translator written by T. Wright[19] and the Tektronix Plot 10 TCS software. The plots are displayed on a Tektronix 4014 display terminal. Typical times required to generate a velocity or a density plot are five to fifteen seconds of CPU time.

B. Linear Heating in an Ambient Homogeneous Fluid

When the ambient fluid is homogeneous, ρ_0 (y) is a constant and Eqs. (13) simplify considerably. For this case it is valuable to examine the analytical form of the solution even though the solution is not calculated for comparison with the numerical results. Several observations about the nature of the flow field can be made from the analytical solution, and these observations are useful discussing the numerical results.

When ρ_0 is constant, the equation for the density in Eqs. (13) can be

solved explicitly using the separable form for Q (x,y,t) given in Eq. (17).

$$\rho(x,y,t) = -\rho_0 D^*(x,y) \int_0^t f(t')\,dt'$$

where

$$D^*(x,y) = \frac{1}{\beta}\lambda\left(\frac{\beta}{\pi}\right)^{1/2}\left\{\exp\left[-\beta(x-x_c)^2-\lambda y\right] - AR\int_0^1 dy' \int_0^{1/AR} \exp\left[-(x'-x_c)^2-\lambda y\right]\right\}$$

and where the density perturbation from ρ_0 is initially taken to be zero. The density is found to be a function of time multiplying a function of space, and density can be expected to display exactly the same spatial behavior at different times with only the amplitude changing from one time to the next.

The velocity field can be decomposed into two fields, one derivable from a potential the other from a stream function:

$$u = \frac{\partial\phi}{\partial x} + \frac{\partial\psi}{\partial y} \quad , \quad v = \frac{\partial\phi}{\partial y} - \frac{\partial\psi}{\partial x}$$

where ϕ is the potential and ψ stream function. The boundary conditions on these two functions arise from the condition that the normal velocity at a boundary be zero (no outflow at a boundary), Eqs. (10): they are $\frac{\partial\phi}{\partial n} = 0$ and $\psi = 0$ on the boundary, $x = 0,\ 1/AR$ and $y = 0,\ 1$ (where $\frac{\partial}{\partial n}$ means the derivative normal to the boundary).

The continuity equation, Eq. (5), implies

$$\nabla^2\phi = D(x,y,t) = f(t)\,D^*(x,y)$$

If we denote by $\Phi(x,y)$ the solution to the equation

$$\nabla^2\Phi(x,y) = D^*(x,y)$$

with $\frac{\partial\Phi}{\partial n} = 0$ at $x = 0,\ 1/AR$ and $y = 0,\ 1$, then

$$\Phi(x,y,t) = f(t)\,\Phi(x,y)$$

We define the vorticity to be

$$\omega \equiv \frac{\partial v}{\partial x} - \frac{\partial u}{\partial y}.$$

Then

$$\nabla^2 \psi = -\omega$$

The equation for the time evolution of the vorticity is obtained by taking the curl of the momentum equations in Eqs. (13)

$$\frac{\partial \omega}{\partial t} = -\frac{1}{\rho_0}\frac{\partial p}{\partial x} = \frac{\partial D^*(x,y)}{\partial x}\int_0^t f(t')\,dt'$$

The solution is

$$\omega = \frac{\partial D^*}{\partial x}\int_0^t dt' \int_0^{t'} dt''\, f(t'')$$

The initial conditions that u (x, y, 0) = v (x, y, 0) = 0 have been used to determine that the initial vorticity distribution is zero.

If, as before, we denote by Ψ (x, y) the solution to the equation

$$\nabla^2 \Psi = -\frac{\partial D^*(x,y)}{\partial x}$$

with Ψ = 0 at x = 0, 1/AR and y = 0, 1, then

$$\psi(x,y,t) = \Psi(x,y)\int_0^t dt' \int_0^{t'} f(t'')\,dt''$$

The point to note from the analytical forms derived above is that the temporal behavior of the velocity field obtained from the potential is different from that obtained from the stream function. In particular, when f (t) grows linearly,

$$f(t) \propto t$$

and

$$\int_0^t dt' \int_0^{t'} dt'' f(t'') \propto \frac{1}{6} t^3 .$$

Hence, initially the potential contribution to the velocity field will dominate and the velocity field will grow approximately linearly with time, whereas later the contribution from the stream function, or rather due to the generation of vorticity, will dominate and the velocities will grow roughly as the cube of time.

In Figure 2 - 6 plots of horizontal and vertical velocity are displayed for a case of heating in an unstratified fluid. The heat source is of the form given in Eq (17) with

$$f(t) = \tanh At$$

Values of the parameters for the heat source shown are $\beta = 24.5$, $\lambda = 4$, $x_c = 0.5$ (cf Eq. (17)) and $A = 0.1$: hence the source is centered along the bottom of the floor, its strength diminishing more rapidly laterally than vertically.

Figure 2 shows, at time $t = 0.1$, horizontal velocity as a function of vertical position at three locations ($x \cong 0.25$, 0.48 and 0.74) and vertical velocity as function of horizontal position at three locations ($y \cong 0.25$, 0.48, 0.74). (Note that the heat source and the flow field are symmetric about the centerline, but the horizontal positions used for plotting are not.) Figure 3 shows the same horizontal and vertical velocity plots at $t = 0.2$. Comparison of these two figures shows that the velocities in Fig. 3 have the same spatial form, but are nearly double those in Fig. 2. At "early time" during the linear calculation,

when these two plots were made, the velocities are dominated by the potential flow as the analysis above indicates. The potential flow represents an expansion of the gas due to heating by the source. At this time the velocities grow linearly with time, and Figs. 2 and 3 confirm this behavior.

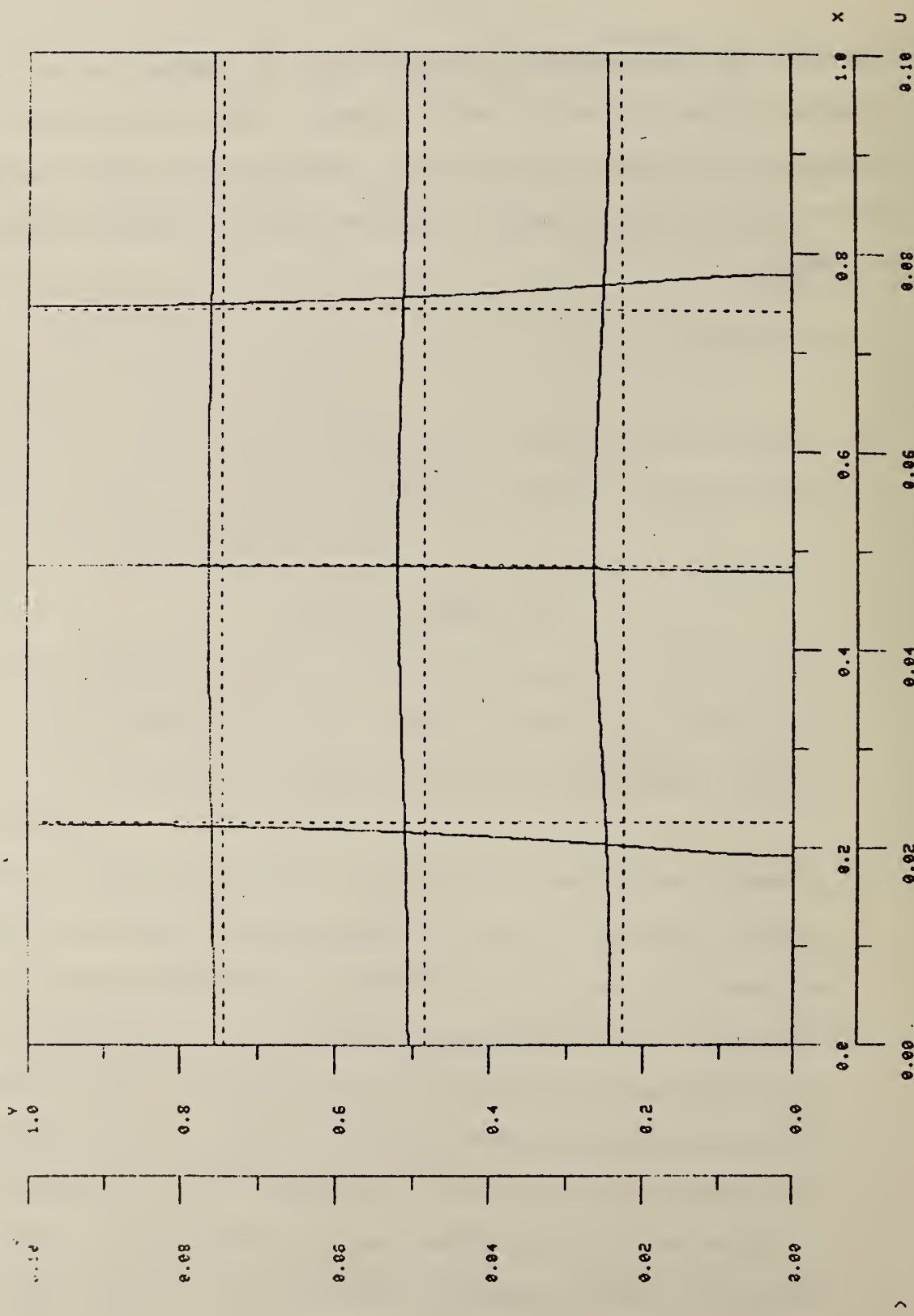
HEATED,UNSTRATIFIED FLUID - LINEAR, CENTERED SOURCE
DATE • 18 OCT 78
TYPE • VELOCITY
T • 1.00000-01
Y
X
U
1.0
0.8
0.6
0.4
0.2
0.0
0.08
0.06
0.04
0.02
0.00
0.10

FIGURE 7

FIGURE 3

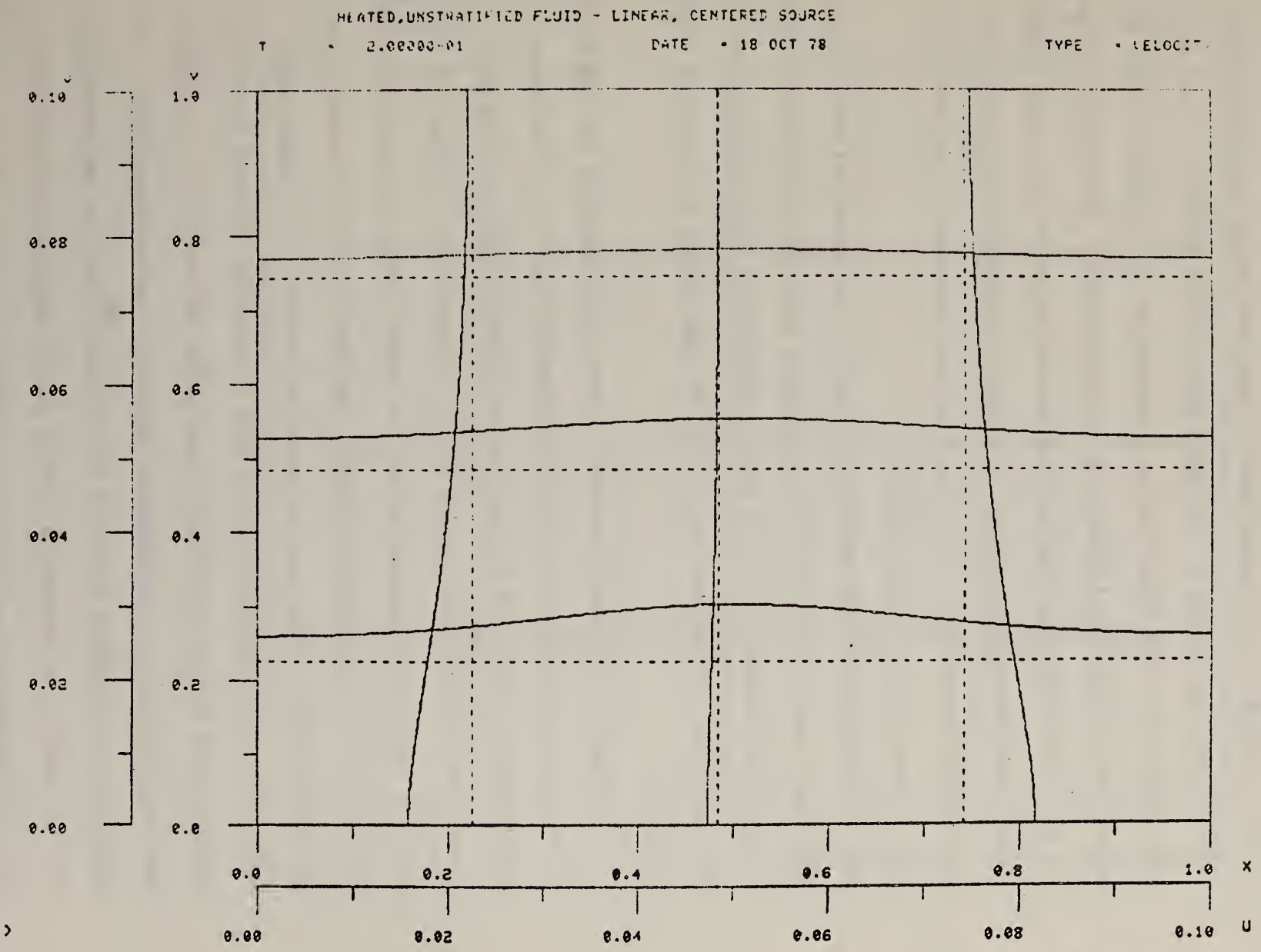
HEATED, UNSTRATIFIED FLUID - LINEAR, CENTERED SOURCE
T = 2.00000-01
DATE = 18 OCT 78
TYPE = VELOCITY
V
0.10
0.08
0.06
0.04
0.02
0.00
1.0
0.8
0.6
0.4
0.2
0.0
0.0
0.2
0.4
0.6
0.8
1.0
X
0.00
0.02
0.04
0.06
0.08
0.10
U

Figures 4 and 5 show these horizontal and vertical velocity plots at t = 2.0 and t = 4.0 respectively. Note the change in the velocity scales from Figs. 2 and 3. At these times, which are "late time" in the linear flow, the flow field is dominated by the vorticity field for which the physical significance is discussed below. The velocity plots in Fig. 5 have the same spatial form but are approximately eight times larger than those given in Fig. 4, a fact consistent with the analysis above, which shows that the stream function (produced by the vorticity field) grows as the cube of time.
are contributions to the velocities from both the potential and the stream function; hence t = 0.7 is an "intermediate time" for the linear calculation in which the velocity field is neither dominated by the potential nor by the vorticity. (Note that Fig. 6 has the same scales for velocity as Figs. 2 and 3.)

An observation should be made at this point regarding the qualitative behavior of the linear flow field exhibited in Figs. 2-6. The overall nature of the flow field is what one would expect (and, for the later times, qualitatively what people find in a room fire). During the "early time" of the linear calculation as noted before (when the velocities are dominated by the potential function), the flow is strictly outward from the heated region as the gas is heated and expands. At "later time" during the linear calculation, the flow is upwardly directed above the heated region and, by continuity, down along the sides of the enclosure. Qualitatively, this is the behavior observed in an enclosure fire. In addition, in the region above the most intensive heating (approximately $y \gtrsim 0.17$ here), the horizontal flow is mildly outwardly directed from the region above the heat source (the plume region). Near the bottom of

FIGURE 4

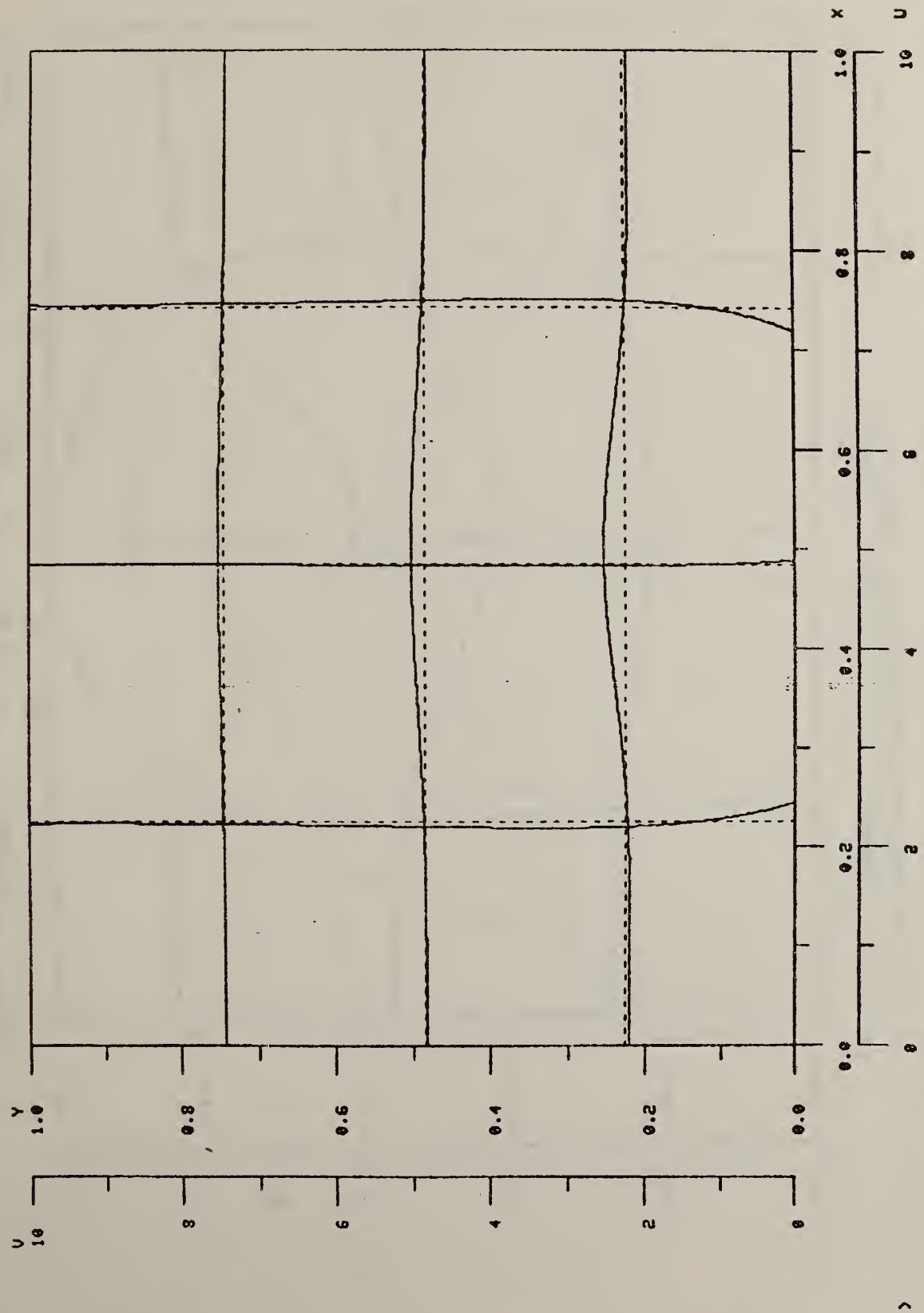
TEST CASE - HEATED,STRATIFIED FLUID - EARLY TIME
T = 2.0000+00
DATE = 10 MAY 78
TYPE = VELOCITY
Y
V
X
U
1.0
0.8
0.6
0.4
0.2
0.0
10
8
6
4
2
0
0.0
0.2
0.4
0.6
0.8
1.0

FIGURE 5

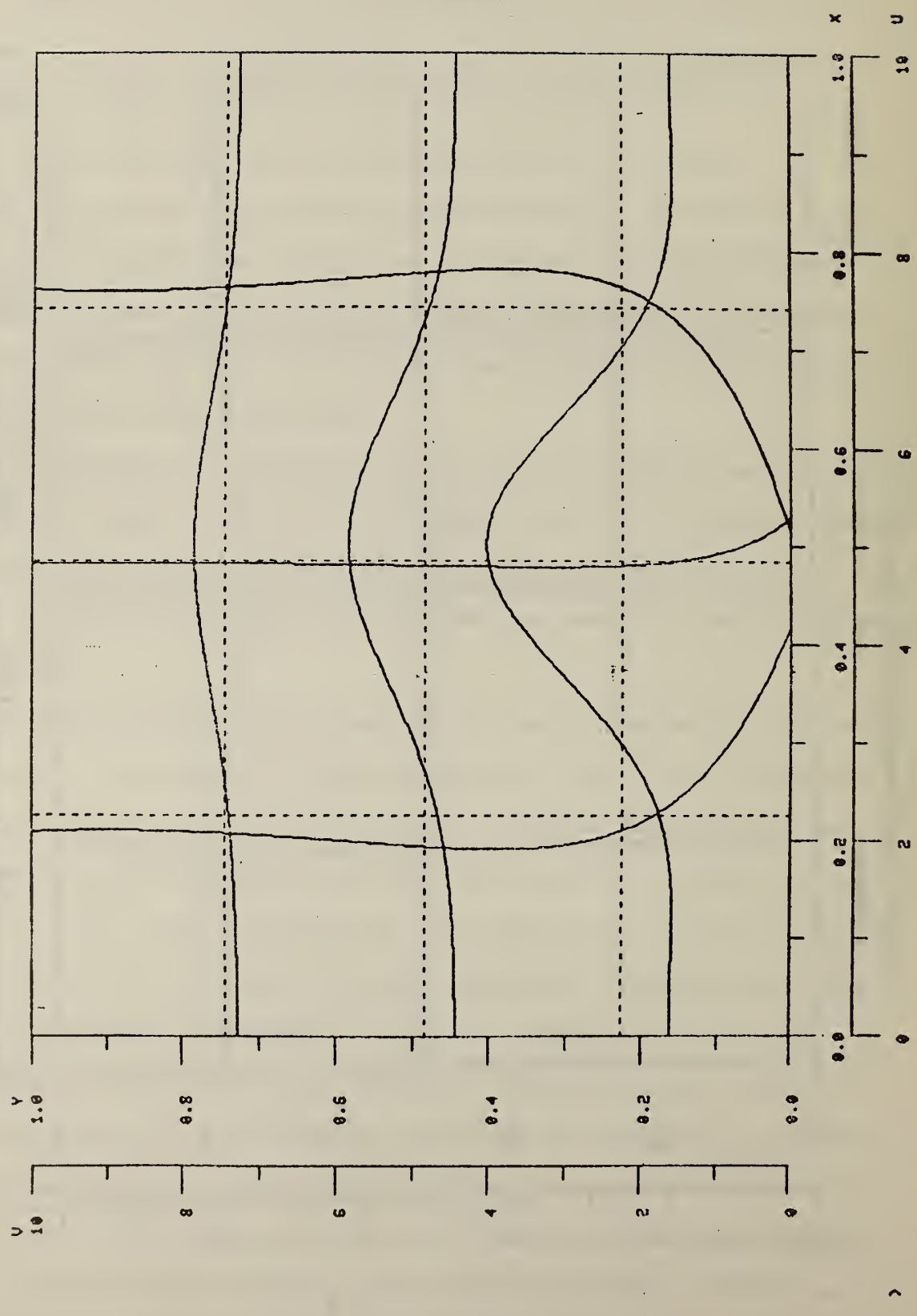
TEST CASE - HEATED,STRATIFIED FLUID - EARLY TIME
T = 4.00000+00
DATE = 10 MAY 78
TYPE = VELOCITY
V
U
X
U

FIGURE 6

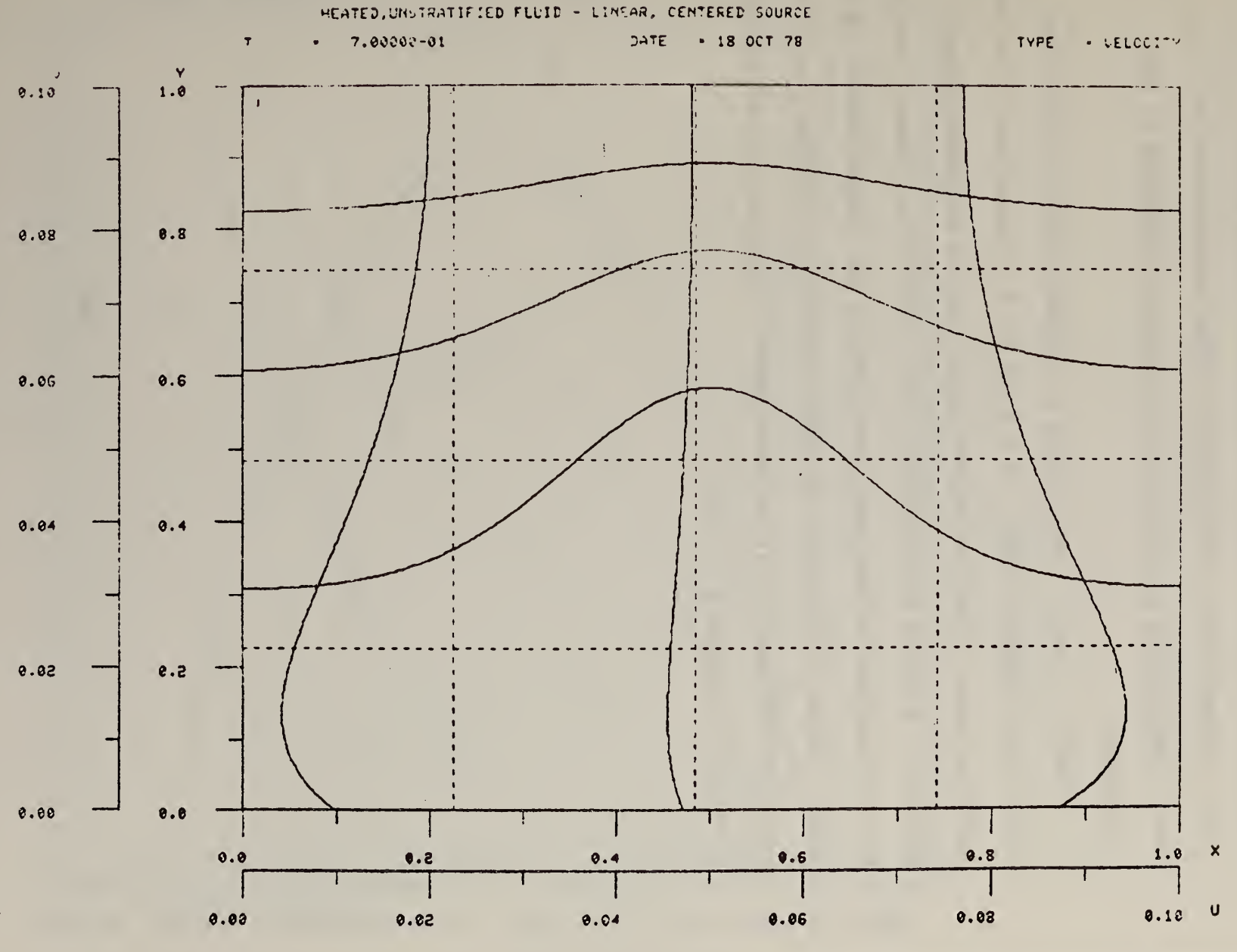
HEATED,UNSTRATIFIED FLUID - LINEAR, CENTERED SOURCE
T = 7.00000-01
DATE = 18 OCT 78
TYPE = VELOCITY
Y
0.10
0.08
0.06
0.04
0.02
0.00
1.0
0.8
0.6
0.4
0.2
0.0
0.0
0.2
0.4
0.6
0.8
1.0
X
0.00
0.02
0.04
0.06
0.08
0.10
U

the enclosure, however, there is a relatively strong inflow. In room fires a strong inflow or "floor jet" is often observed near the floor. Such a qualitatively good picture from a linear calculation is very encouraging.

Finally, in Figs. 7 and 8 plots of constant-density contours are shown at two different times, t = 0.5 and t = 2.0 respectively. Two points should be noted. First, as observed above from the analytical solution, the spatial behavior of the density at the two different times is the same, only the magnitude of the density perturbation has changed between the two times. Second, we note that the spatial behavior of the density perturbation is proportional to D (x, y) and hence directly reflects the nature of the specified heat source Q (x, y).

FIGURE 7

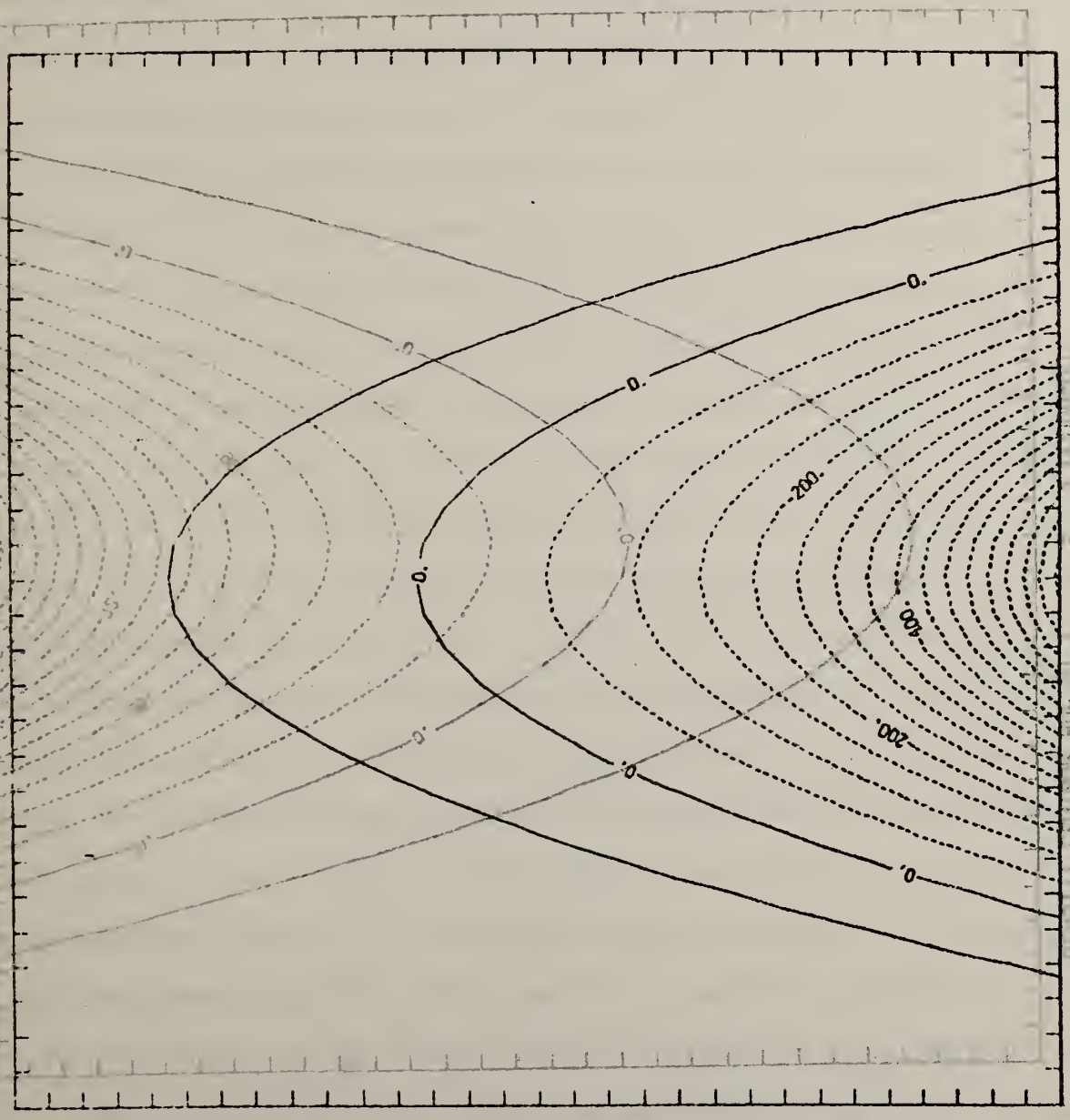
DENSITY CONTOUR MAP AT I = 5.0000-01
0.
200.
400.
CONTOUR FROM -.80000-01 TO .50000-02 CONTOUR INTERVAL OF .50000-02 PTS(3,3)= .74669-02 LABELS SCALED BY 10000.

FIGURE 8

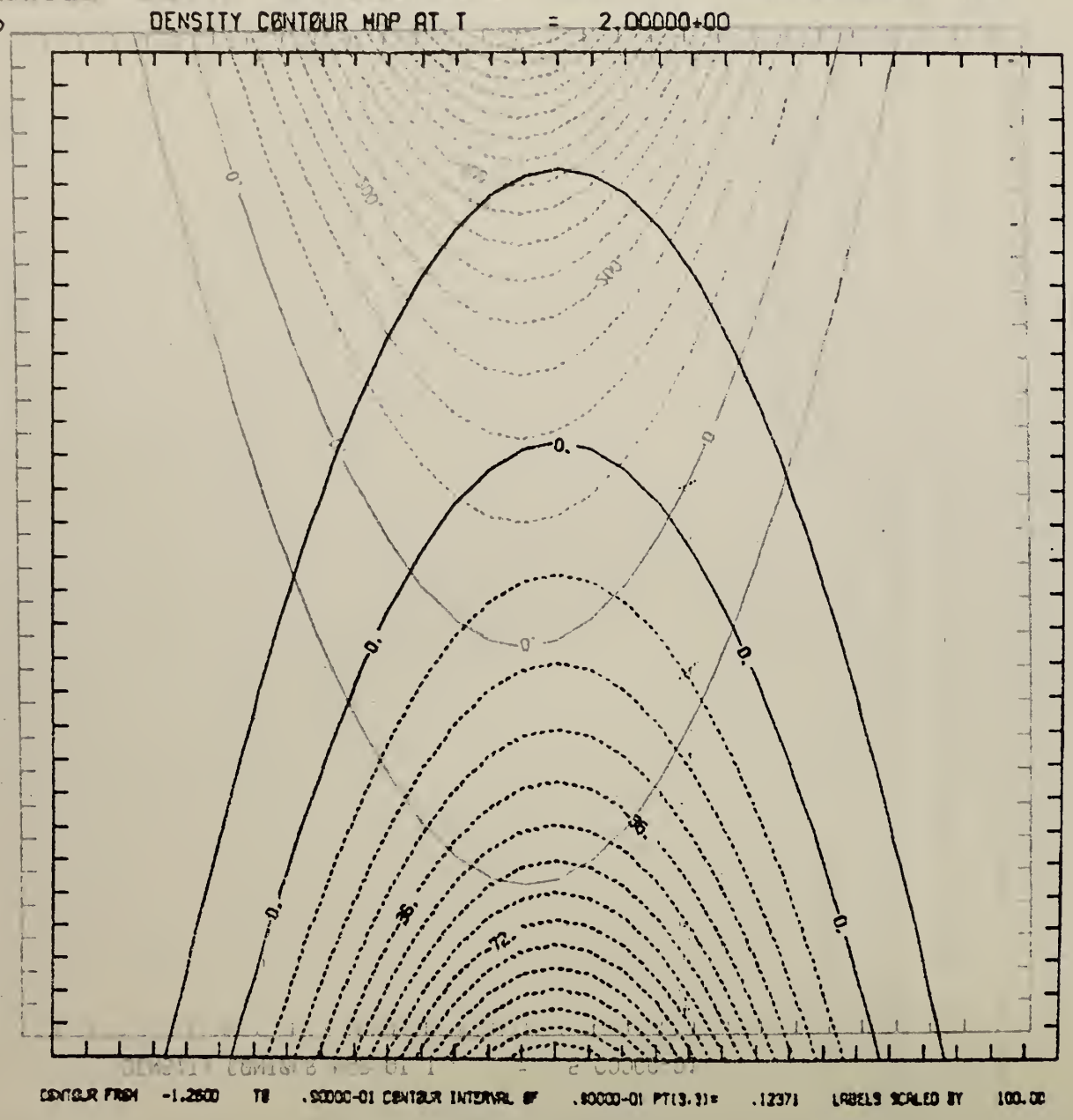

FIGURE 9

C. Linear Heating in a Stratified Fluid

When the ambient fluid is stratified with an exponential variation as given in Eq. (16a), a formal solution to Eqs. (13) can still be obtained (because the equations are linear). However, because of the complexity of this solution, it is not very helpful for gaining an understanding of the behavior of the flow field. Therefore, in this section results of some computations solving the complete difference equations, Eqs. (19) and (21), will be presented and discussed, but no additional analysis will be presented.

In all of the computations reported in this section, a reasonably refined mesh, I = J = 31, was chosen. The enclosure was taken to be a square, $A_r = 1.0$, and the gas constant $\gamma = 1.4$. Parameters describing the heat source were $\beta = 24.5$, $\lambda = 4.0$ in Eqs. (19) and $A = 0.1$ in Eqs. (20). The parameter ε, specifying the relative error to which the pressure equation is to be solved, was taken to be 10^{-5}, and the dimensionless time step was taken to be $\delta t = 0.2$. All other parameters relevant to the individual computations reported will be stated when the results are discussed.

An interesting observation can be made at this point regarding the relative effort required to obtain numerical solutions (in the form of plots say) as the complexity of the (linear) problem increases. In a previous paper, Ref. 10, the authors obtained solutions to the equations for internal waves in enclosures. In the continuous case, these waves are solutions to the homogeneous form of Eqs. (13), and in the discrete case, they are solutions to the homogeneous forms of Eqs. (19) and (21). Analytical solutions to both the continuous and the discrete cases were obtained, and a numerical solution was also obtained by the time-stepping procedure described in this report. To generate a code and compute numerical values for the homogeneous

problem was very simple using the analytical solutions, but required much effort for the direct numerical time-stepping procedure. Once the time-stepping procedure was implemented as a code, it was a easy task to modify it to calculate the inhomogeneous problems with constant or variable ambient density (described in the last section and this section respectively). To calculate values from the analytical solution to the inhomogeneous problem with constant background density in the continuous case requires some effort, but not too much. However, to perform a similar task when the background density is variable is a rather big effort. In short, as the complexity of the problem, even though linear, increases, the effort required to obtain and evaluate analytical results may become much greater than straightforward numerical integration by difference methods. In the nonlinear case, of course, analytical solution will not even be possible.

C.1. Heating in a Stratified Fluid by a Centered Heat Source

Internal waves can be sustained in a stratified fluid. As noted above these waves are solutions to the homogeneous form of Eqs. (13). The heating source is the inhomogeneous, driving term for these equations, and this source excites internal waves during heating. One of the most interesting features of the plots shown in this and the subsequent two examples in this section are the internal waves generated by the heat source. With each of the examples other observations will be made.

In this first example the stratification parameter $Y_s = 1.0$. Hence the buoyancy period $T \equiv 2\pi \left(-g\frac{d\rho_e}{dy}\frac{1}{\rho_0}\right)^{1/2} = 2\pi / Y_s^{1/2} = 2\pi$, and to observe any effects of internal waves, the calculations must be performed for at least a period or two. This computation was run for 14 dimensionless time units with $\delta t = 0.2$ so that 70 time steps were taken.

In Fig. 9 plots of horizontal and vertical velocities at dimensionless time t = 4.0 for this case are presented. These plots should be compared with those presented in Fig. 5: qualitatively, the plots are the same. However, some quantitative differences can be observed. First, all velocities are somewhat smaller in Fig. 9 (the stratified fluid) than in Fig. 5; the difference is particularly noticable in the vertical velocities. This effect is directly traceable to the stable background stratification which tends to suppress buoyant vertical velocities induced by the heating. Another difference appears in the horizontal velocities where the transition between outflow from the center of the heated region and inflow occurs lower in the enclosure due to the background stratification.

The next three figures, Figs. 10, 11 and 12, show the subsequent development with time (t = 8.0, 12.0 and 14.0 respectively) of the velocity profiles. Note the change in the velocity scales from Fig. 5. It appears from these plots that the vertical velocity changes little in magnitude over the time period represented. However, the horizontal velocities change substantially during this period. The maximum horizontal velocity increases with time and the transition between outflow from the center of the heat source to inflow occurs lower in the enclosure at each time. Other distortions of the profiles as functions of time are also apparent, and these changes are a result of the background stratification.

The nature of the internal-wave effects can be seen more clearly in plots of the density perturbation (from the background exponentially varying density) at times t = 2.0, 4.0, 8.0 and 12.0 in Figs. 13 - 16. In Fig. 13 constant perturbation-density contours at t = 2.0 are shown: clearly these are qualitatively very similar to the perturbation density contours for the unstratified case shown in Figs. 7 and 8. However, at later times the

density contours become qualitatively quite different, the most dominant feature at any single time being that these contours are dramatically flattened. Internal-wave effects become apparent by comparing plots at different times. Such comparison shows that the point (or points) of highest density, denoted by the letter H, sloshes back and forth within the enclosure. Furthermore, examination of the zero-perturbation contour shows undulations with increasing time.

FIGURE 9

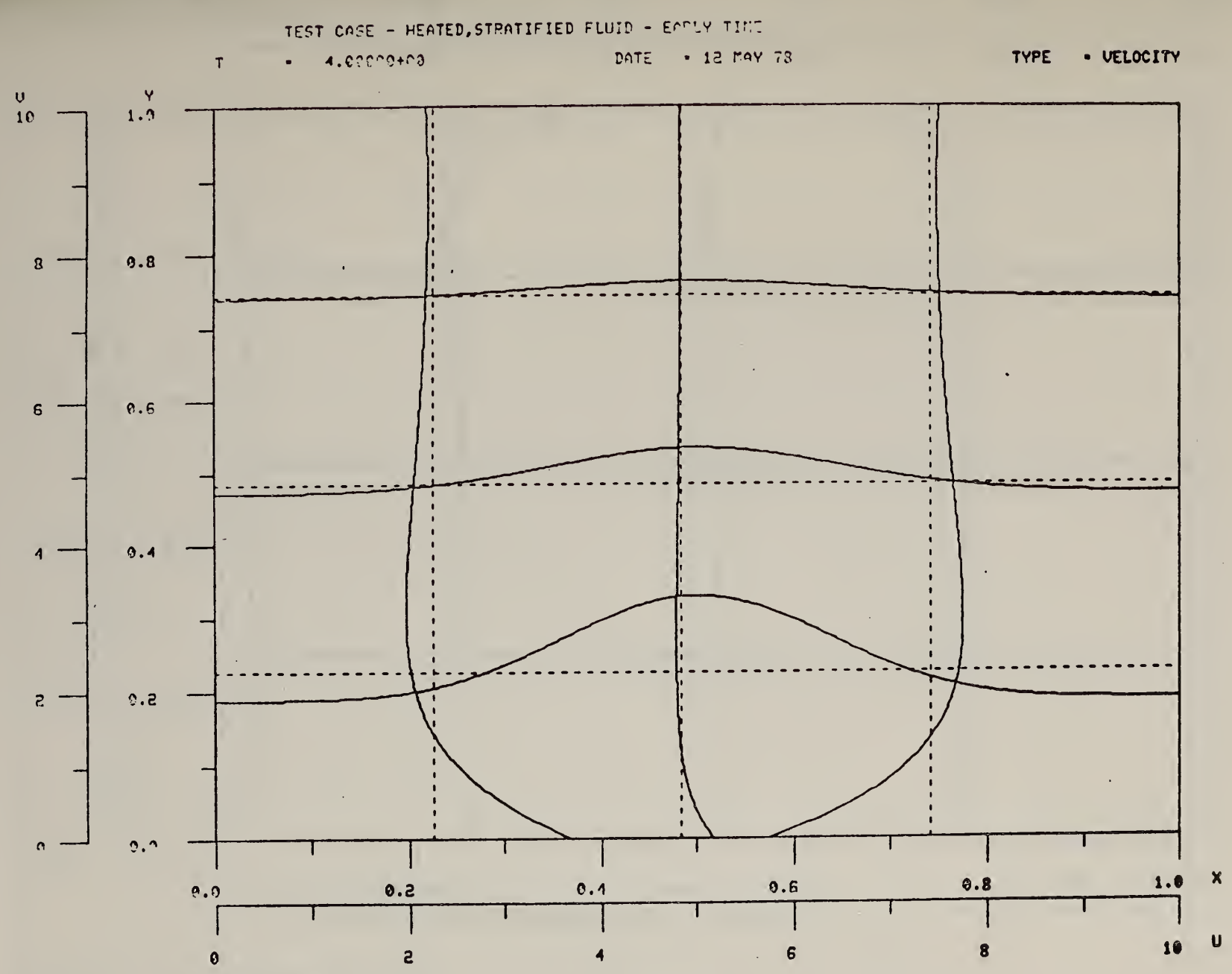
TEST CASE - HEATED,STRATIFIED FLUID - EARLY TIME
T = 4.00000+00
DATE = 12 MAY 78
TYPE = VELOCITY
U
Y
10
8
6
4
2
0
1.0
0.8
0.6
0.4
0.2
0.0
0.0
0.2
0.4
0.6
0.8
1.0
X
0
2
4
6
8
10
U

FIGURE 10

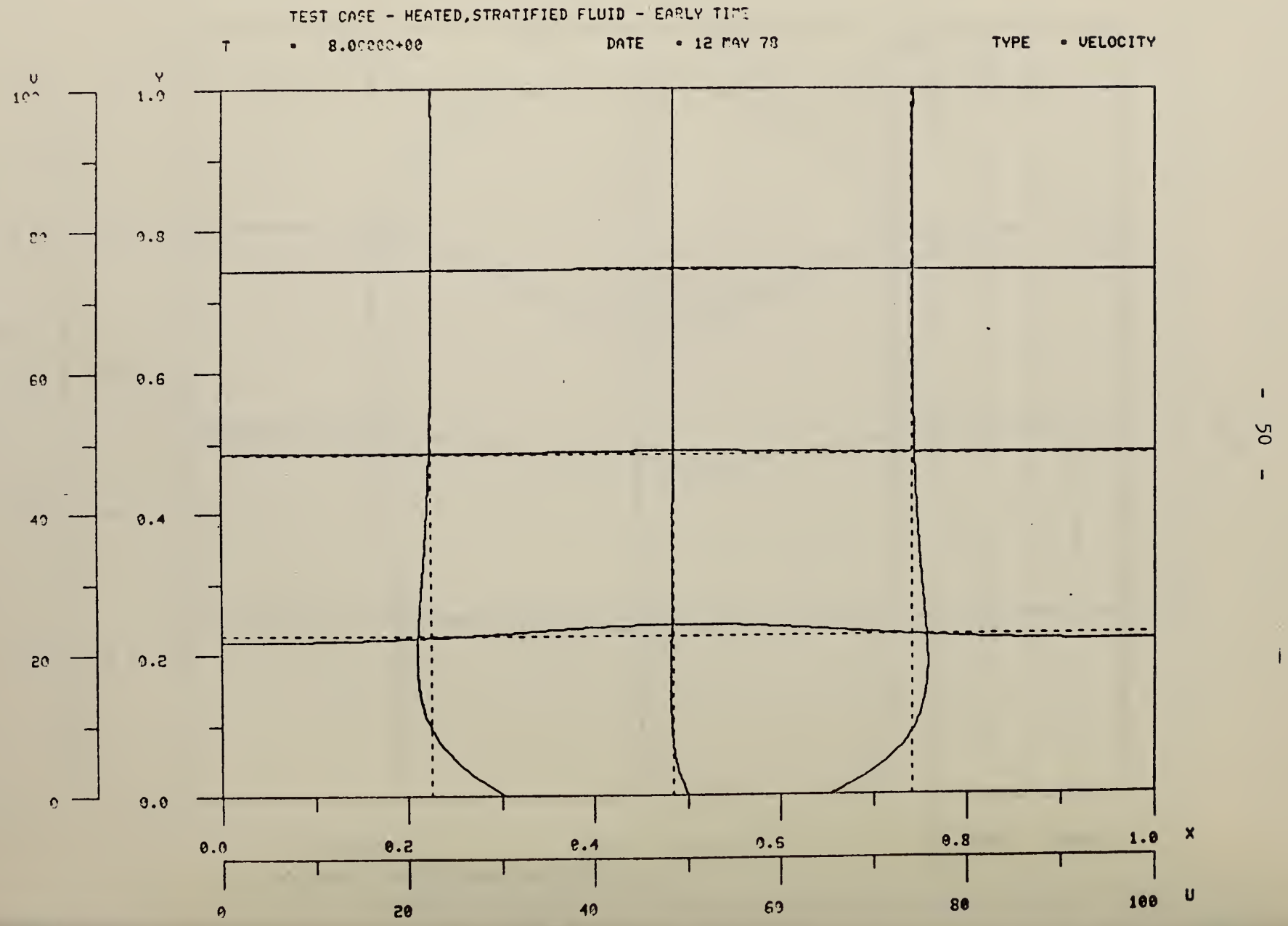
TEST CASE - HEATED,STRATIFIED FLUID - EARLY TIME
T • 8.00000+00
DATE • 12 MAY 78
TYPE • VELOCITY
U
Y
1.0
0.8
0.6
0.4
0.2
0.0
0.0
0.2
0.4
0.6
0.8
1.0
X
0
20
40
60
80
100
U

FIGURE 11

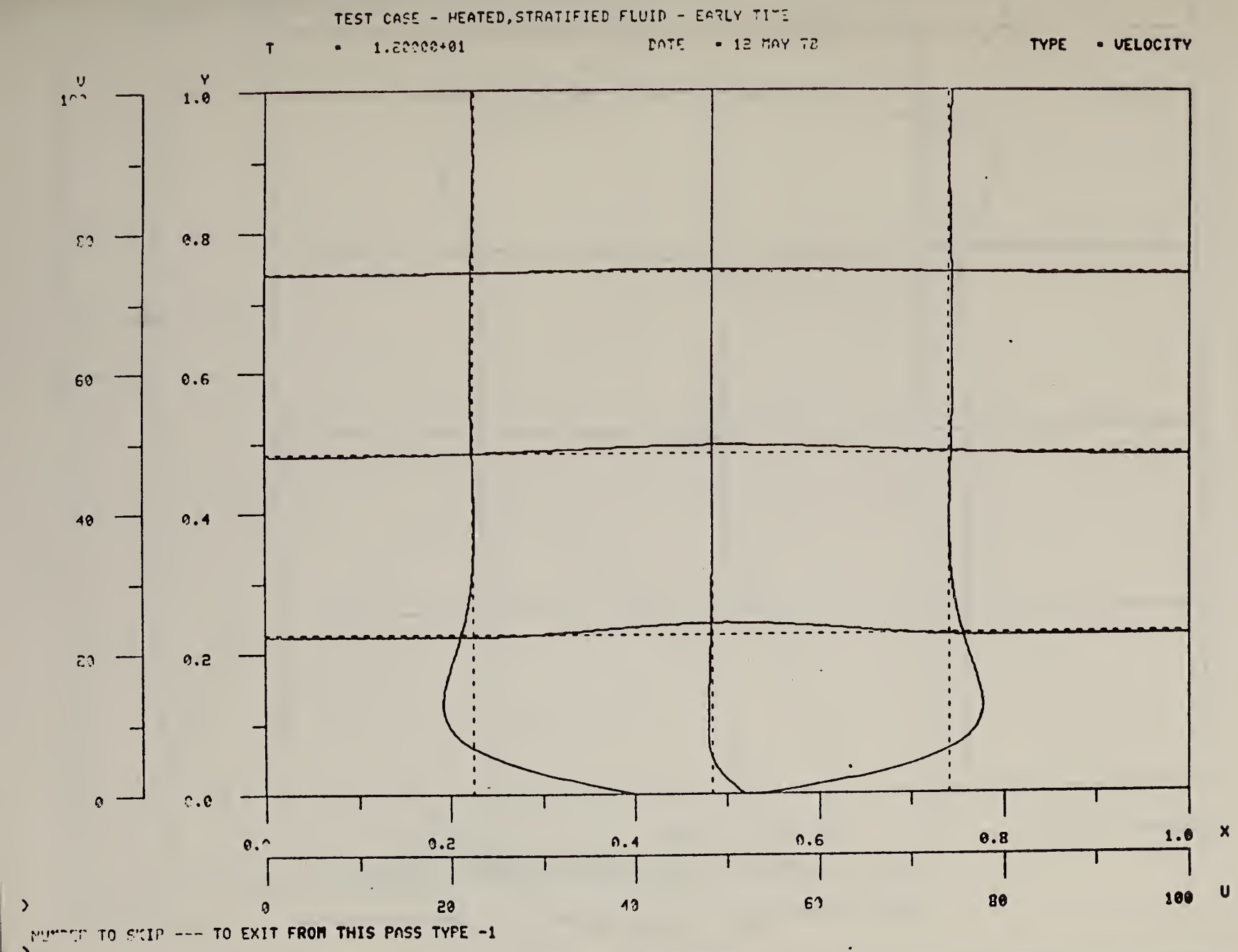
TEST CASE - HEATED,STRATIFIED FLUID - EARLY TIME
T • 1.20000+01
DATE • 12 MAY 72
TYPE • VELOCITY
U
Y
1.0
0.8
0.6
0.4
0.2
0.0
80
60
40
20
0
0.2
0.4
0.6
0.8
1.0
X
0
20
40
60
80
100
U
NUMBER TO SKIP --- TO EXIT FROM THIS PASS TYPE -1

FIGURE 12

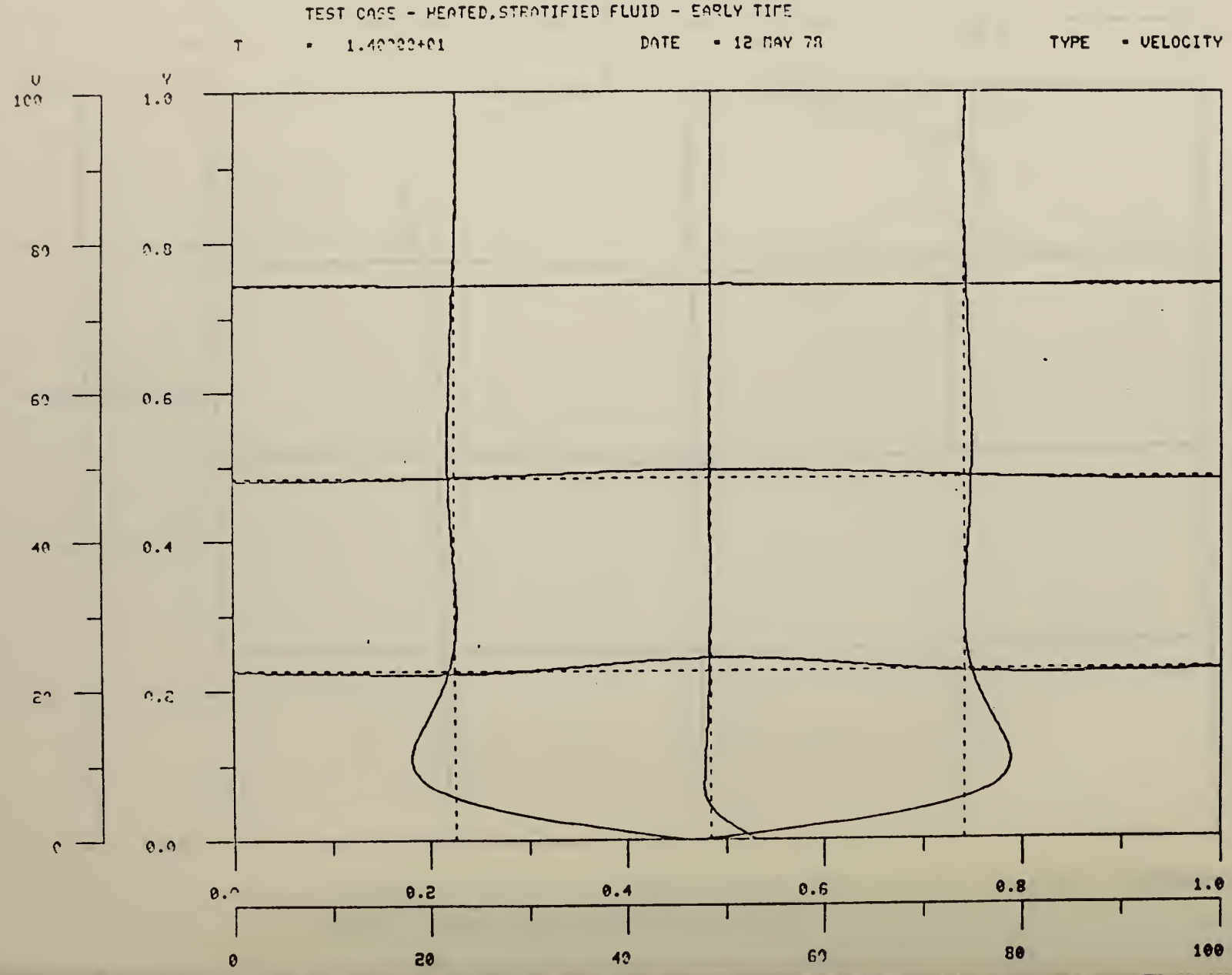
TEST CASE - HEATED,STRATIFIED FLUID - EARLY TIME
T = 1.40000+01
DATE = 12 MAY 78
TYPE = VELOCITY
U
100
80
60
40
20
0
Y
1.0
0.8
0.6
0.4
0.2
0.0
0.0
0.2
0.4
0.6
0.8
1.0
X
0
20
40
60
80
100
U

FIGURE 13

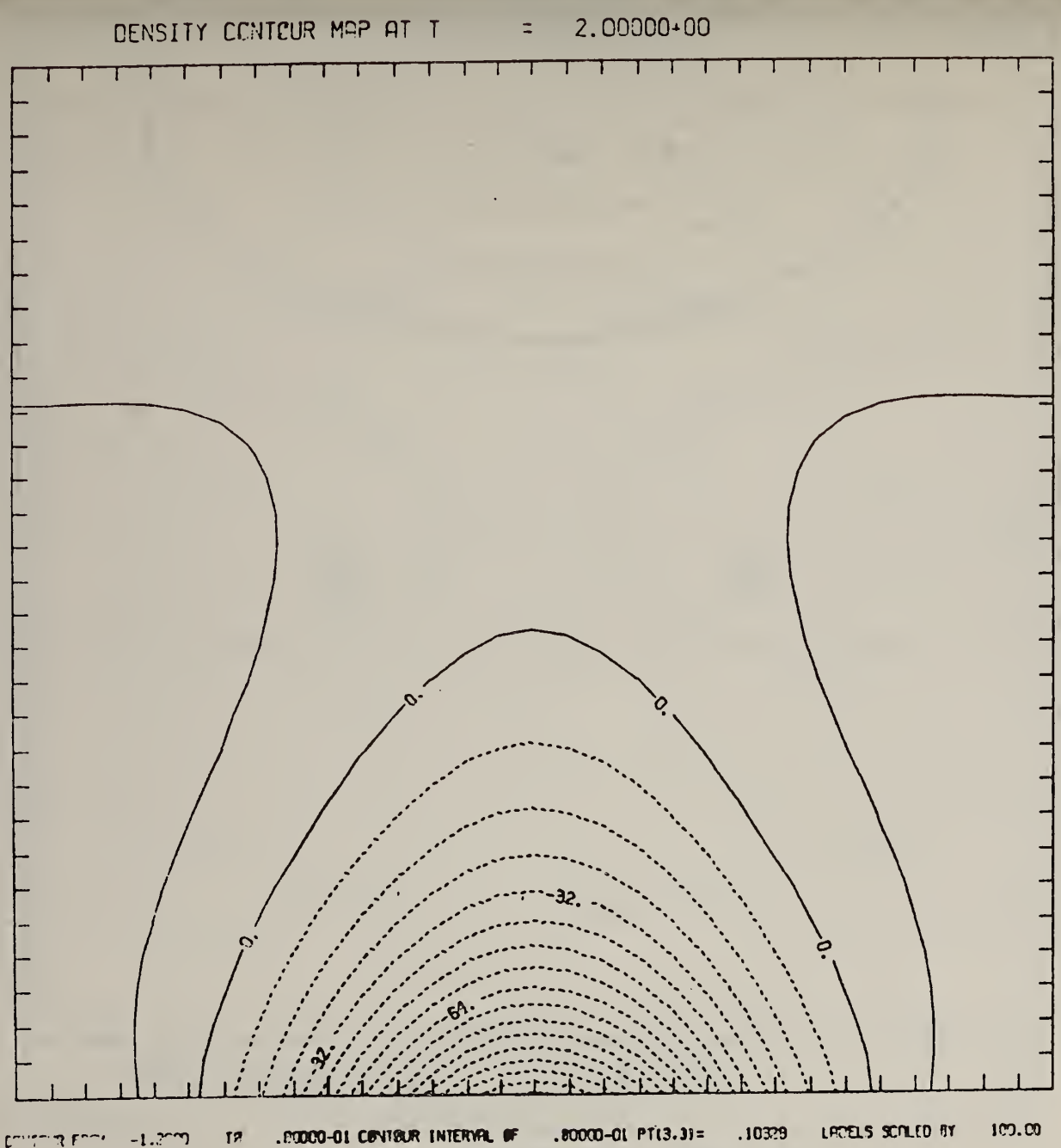
DENSITY CONTOUR MAP AT T = 2.00000+00
0.
0.
0.
0.
-32.
-64.
-96.
.00000-01 CONTOUR INTERVAL OF .00000-01 PT(3.3)= .10329 LABELS SCALED BY 100.00

FIGURE 14

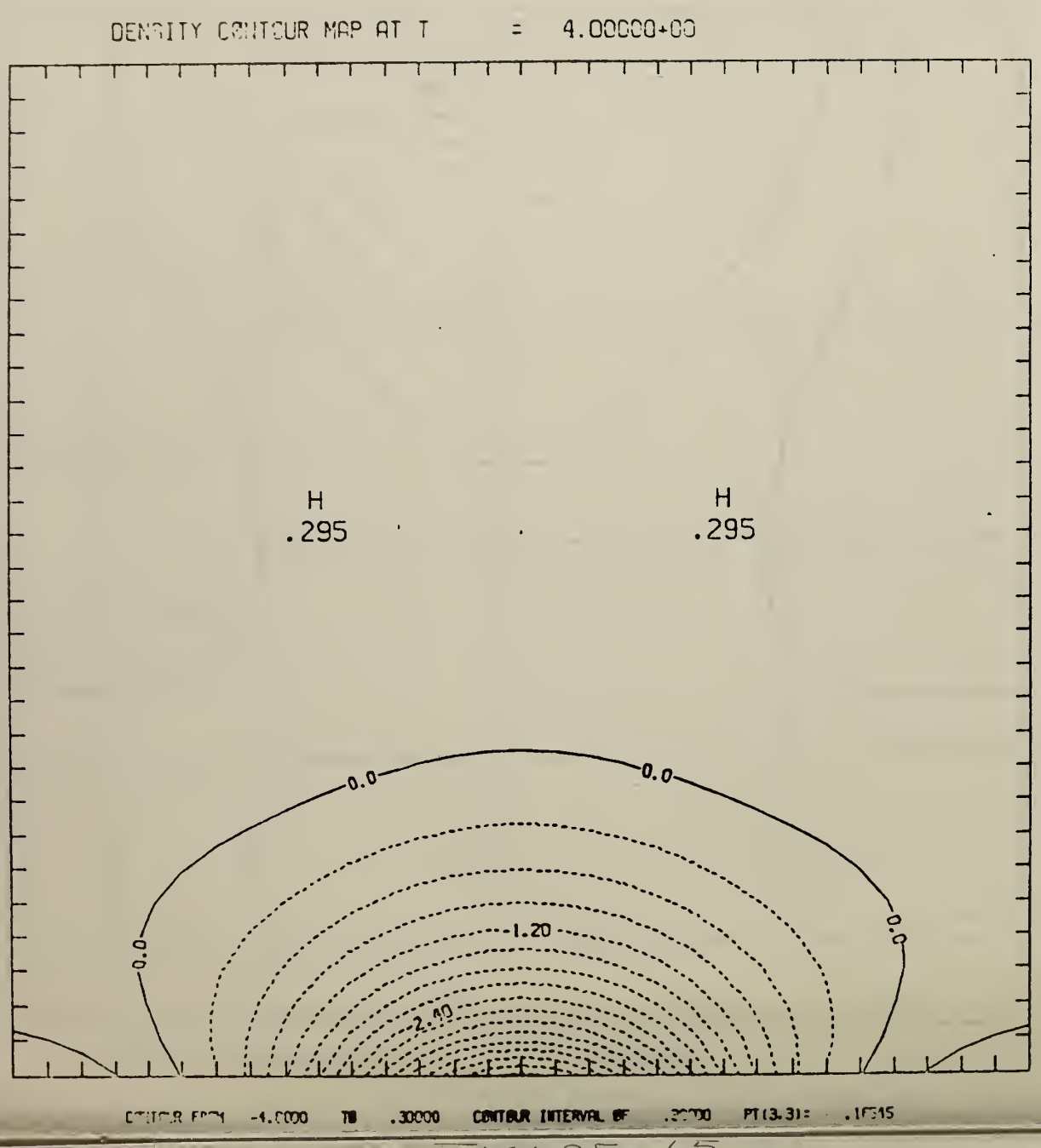
DENSITY CONTOUR MAP AT T = 4.00000+00
H
.295
H
.295
0.0
0.0
0.0
0.0
-1.20
-2.40
CONTOUR FROM -4.0000 TO .30000 CONTOUR INTERVAL OF .30000 PT(3,3)= .10515

FIGURE 15

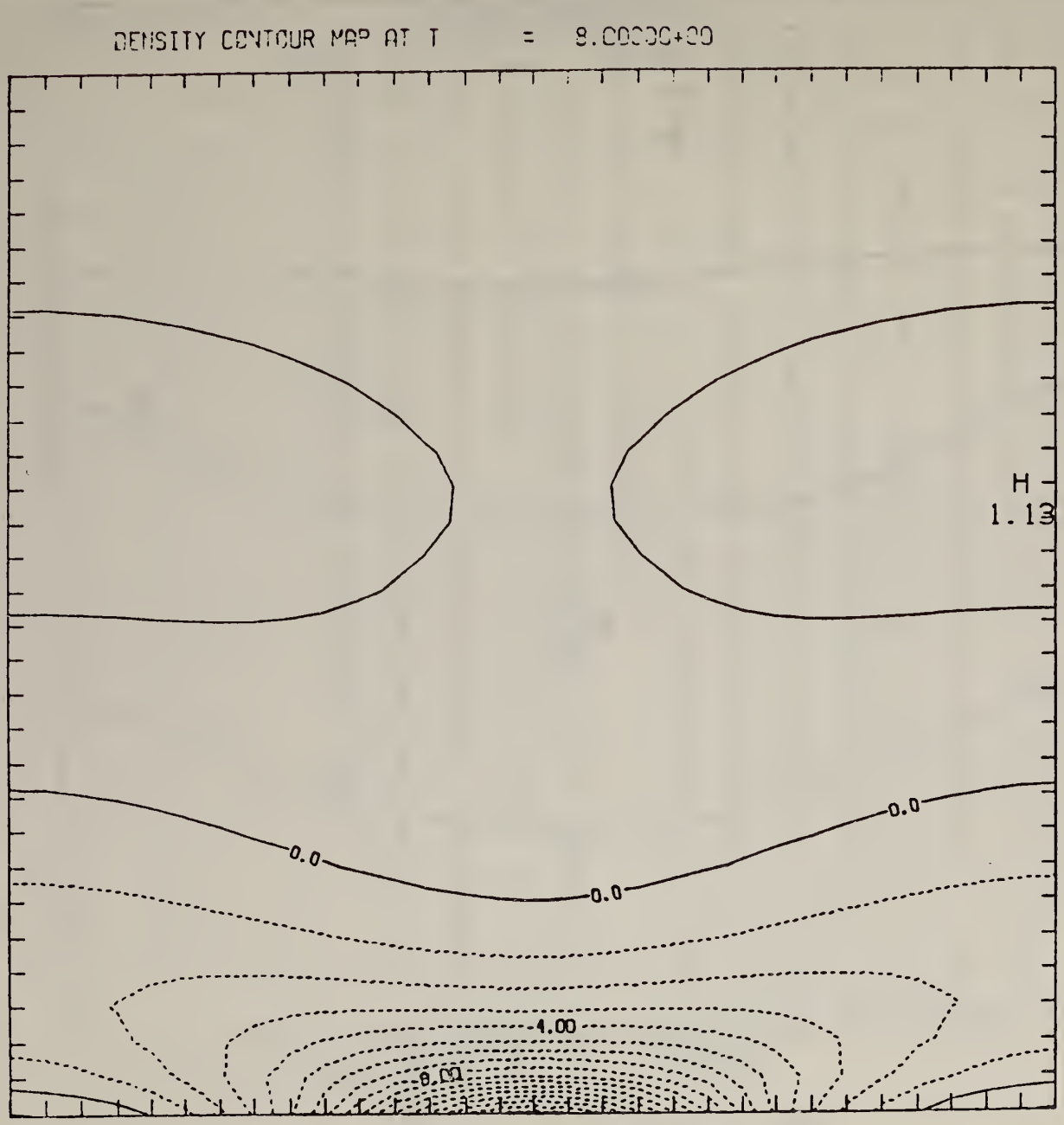
DENSITY CONTOUR MAP AT T = 8.00000+00
H
1.13
0.0
0.0
0.0
-4.00
-8.00
CONTOUR REF -16.000 TO 1.0000 CONTOUR INTERVAL OF 1.0000 PT(3,3)= -1.5000

FIGURE 16

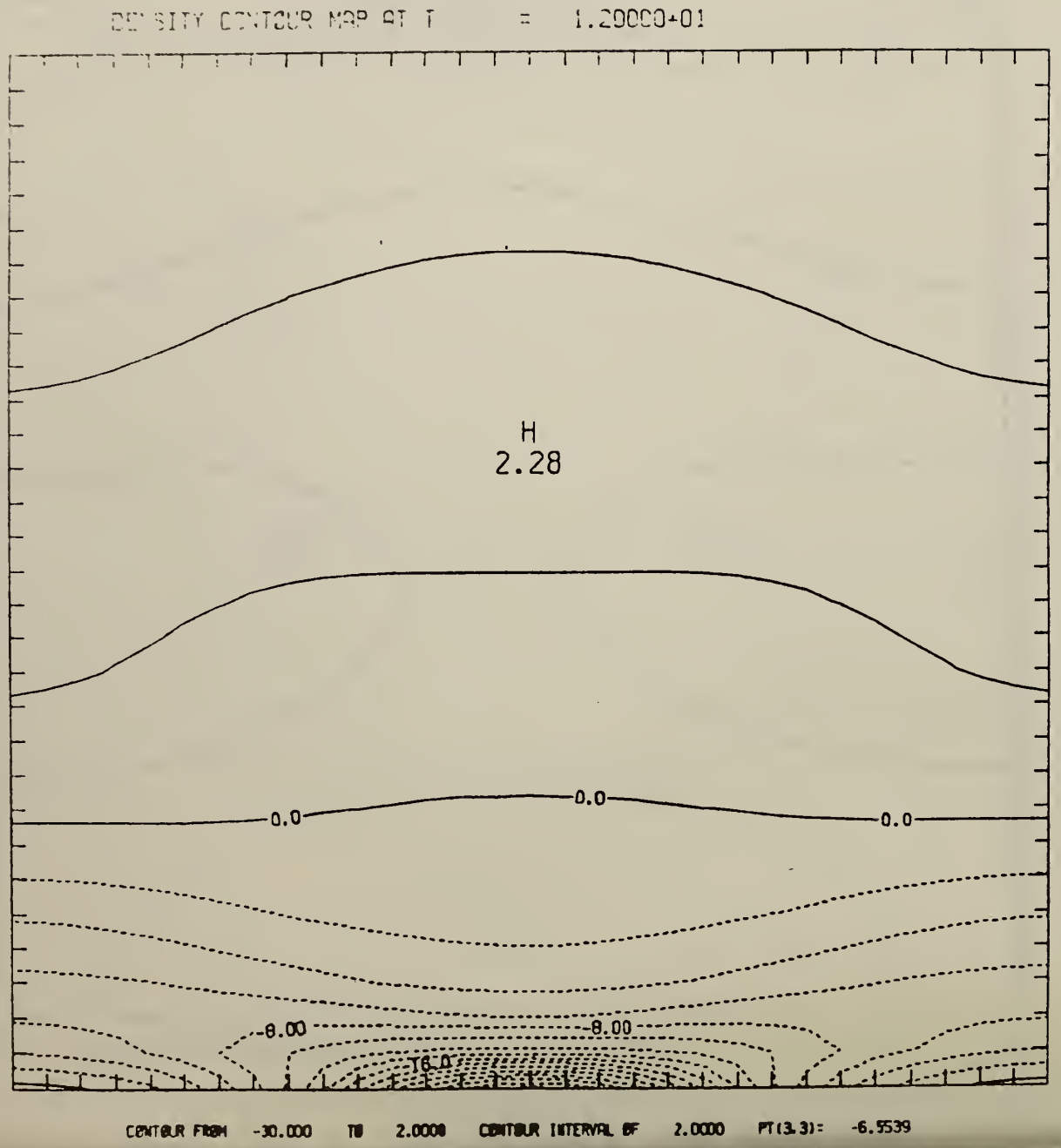
DENSITY CONTOUR MAP AT T = 1.20000+01
H
2.28
0.0
0.0
0.0
-8.00
-8.00
-6.0
CONTOUR FROM -30.000 TO 2.0000 CONTOUR INTERVAL OF 2.0000 PT(3,3)= -6.5539

C.2. Heating in a Stratified Fluid by a Noncentered Heat Source

In this calculation the center of the heat source was shifted to $x = 0.306$ (compared with $x = 0.5$ in previous calculations). All other parameters remained the same as in previous calculations, and the computation was run for 70 time steps, or to $t = 14.0$.

Figures 17, 18 and 19 show velocity profiles at $t = 4.0$, 8.0 and 12.0 respectively. (Note the change of scale of the plots between Fig. 17 and Fig. 18.) The most distinguishing feature of these plots (and of this calculation) is the asymmetry introduced by this noncentered heat source. As in the previous case, the magnitude of the vertical velocities change little, but the shape of these plots change somewhat as functions of time. The horizontal velocity profiles change both in magnitude and in shape as functions of time. The locations of the transitions between outflow from the center of the source to inflow change as functions of time, occuring lower in the enclosure as time increases.

Figures 20 - 23 show constant-perturbation density contours at $t = 2.0$, 4.0, 8.0 and 14.0 respectively. At $t = 2.0$, these contours are qualitative similar, although displaced in the enclosure because of the noncentered heat source, to those shown in Fig. 13. At later times the contours become flattened, and undulations, as described in the previous case, occur.

FIGURE 17

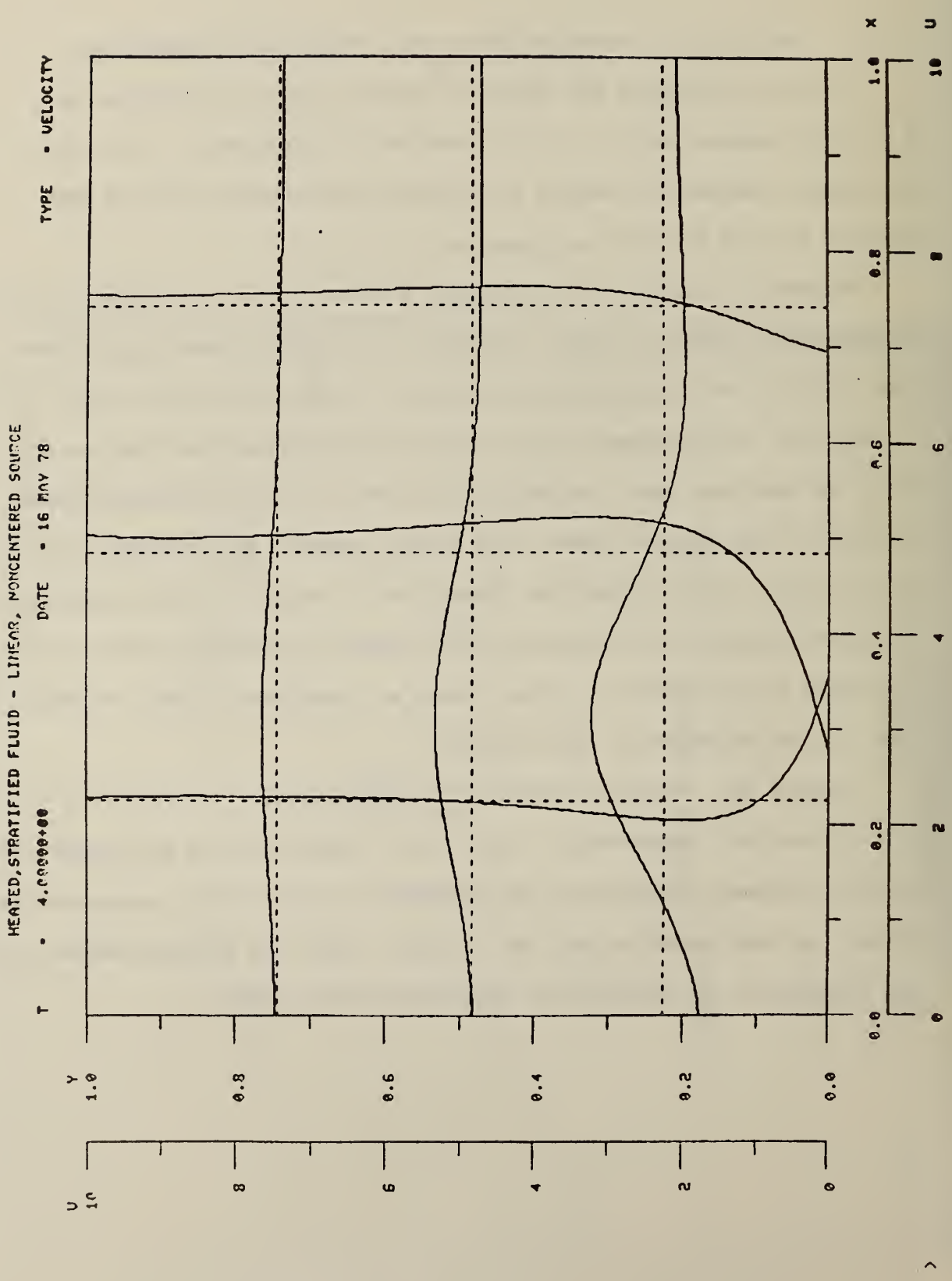
HEATED,STRATIFIED FLUID - LINEAR, NONCENTERED SOURCE
T = 4.00000+00
DATE = 16 MAY 78
TYPE = VELOCITY
Y
1.0
0.8
0.6
0.4
0.2
0.0
U
10
8
6
4
2
0
X
0.0
0.2
0.4
0.6
0.8
1.0
U
0
2
4
6
8
10

FIGURE 18

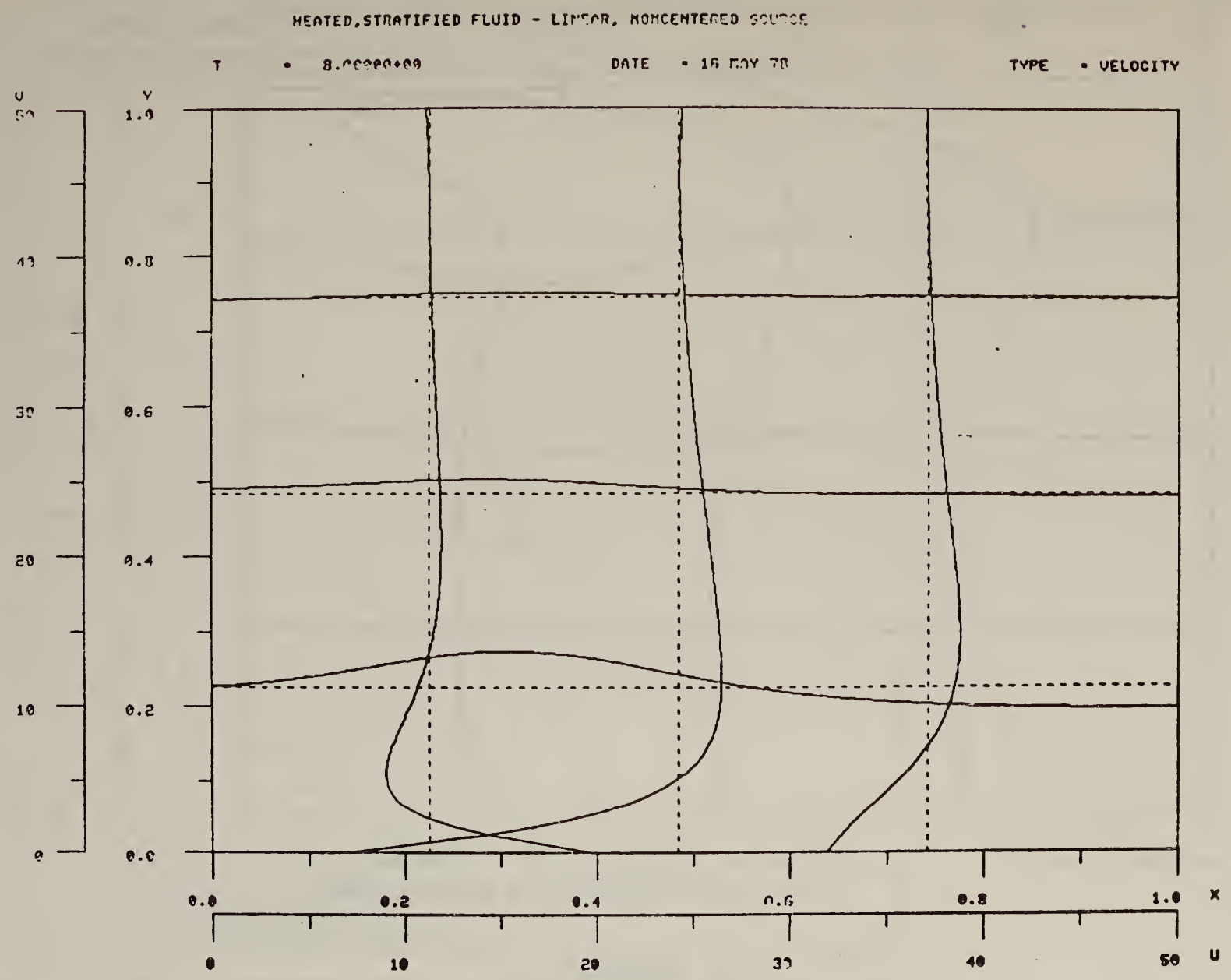
HEATED,STRATIFIED FLUID - LINEAR, NONCENTERED SOURCE
T = 8.0000+00
DATE = 16 MAY 78
TYPE = VELOCITY
U
Y
50
40
30
20
10
0
1.0
0.8
0.6
0.4
0.2
0.0
0.0
0.2
0.4
0.6
0.8
1.0
X
0
10
20
30
40
50
U

FIGURE 19

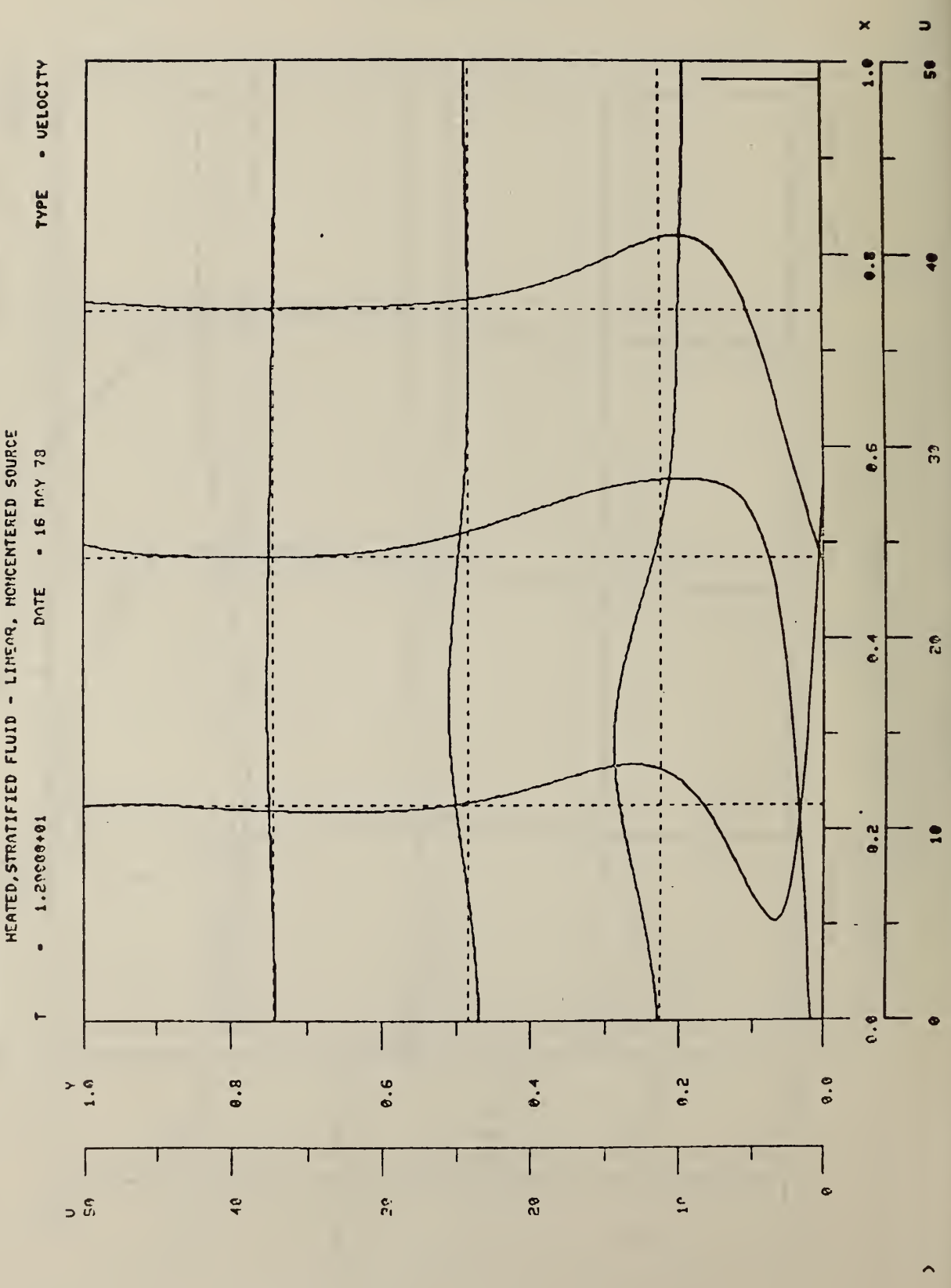
HEATED,STRATIFIED FLUID - LINEAR, NONCENTERED SOURCE
T = 1.20000+01
DATE = 16 MAY 78
TYPE = VELOCITY
Y
X
U
0.0
0.2
0.4
0.6
0.8
1.0
0
10
20
30
40
50

FIGURE 20

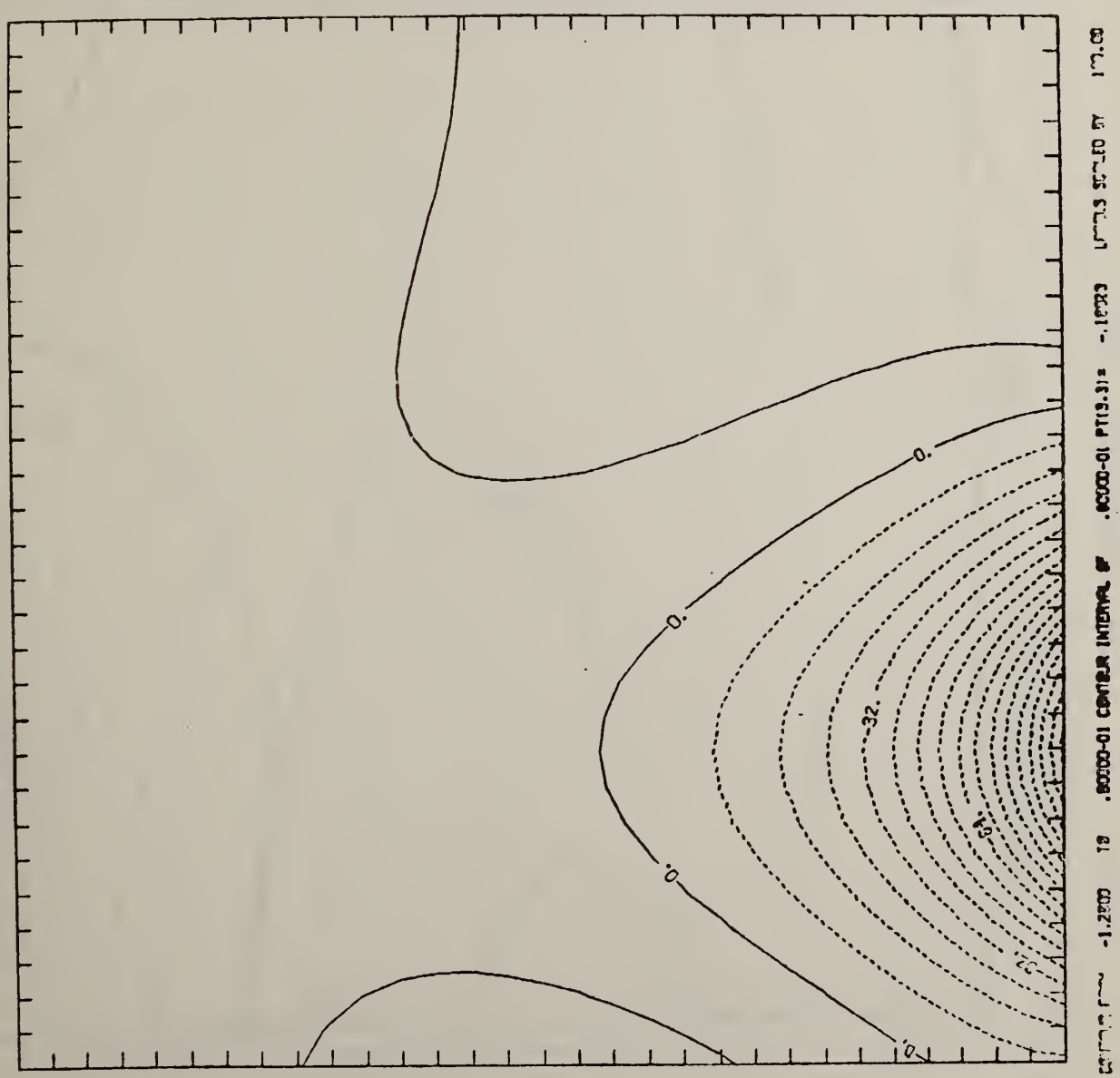

FIGURE 21

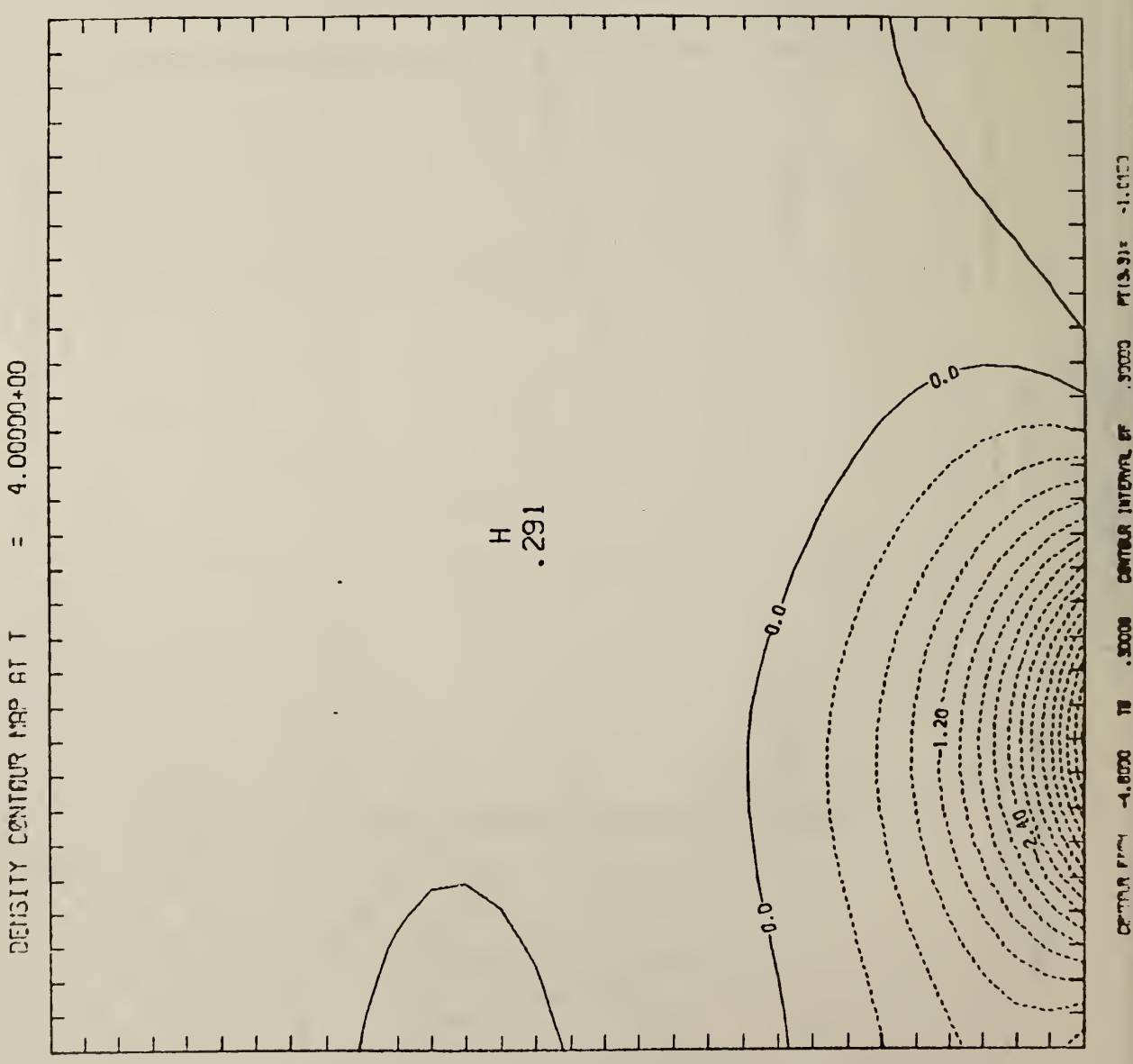

FIGURE 22

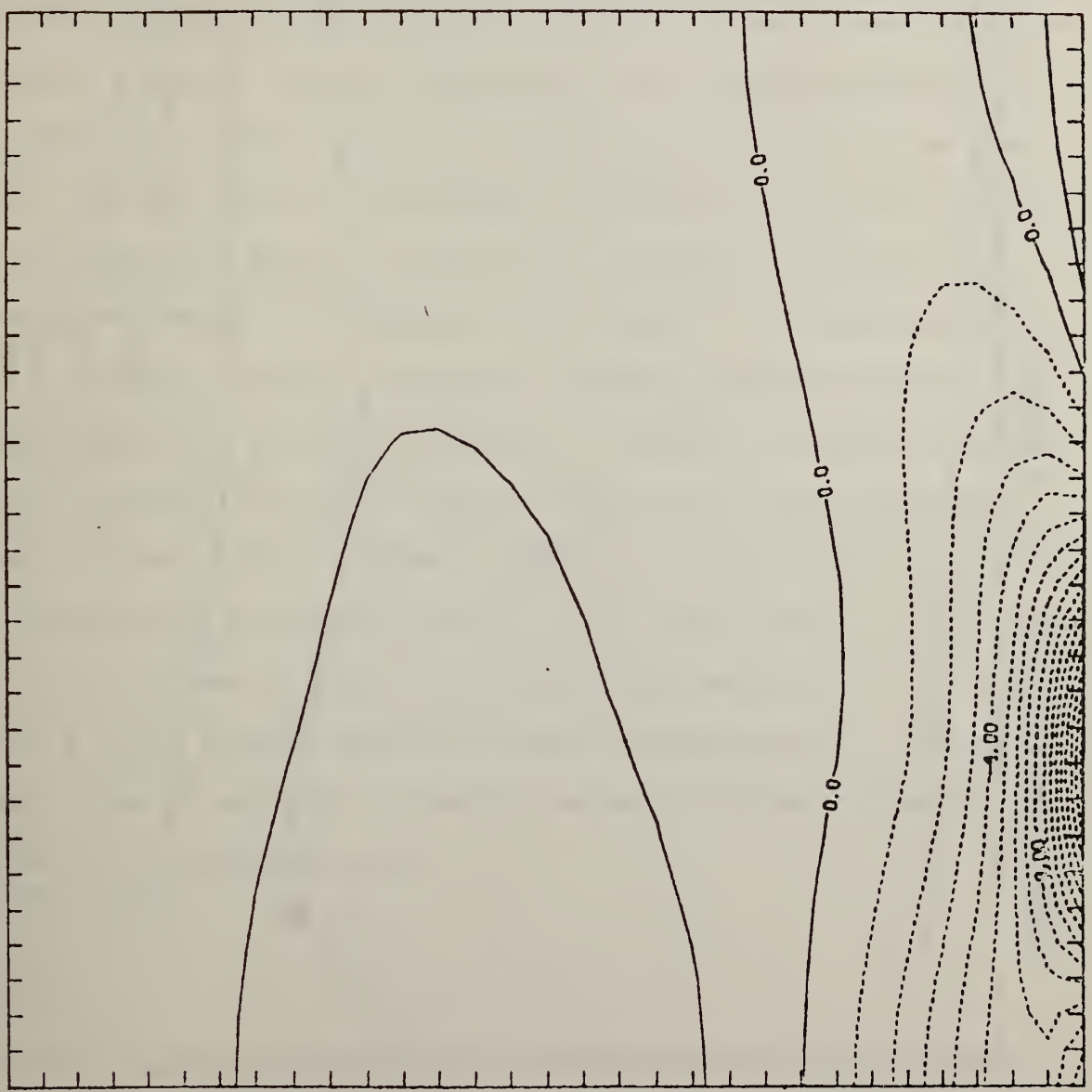

FIGURE 23

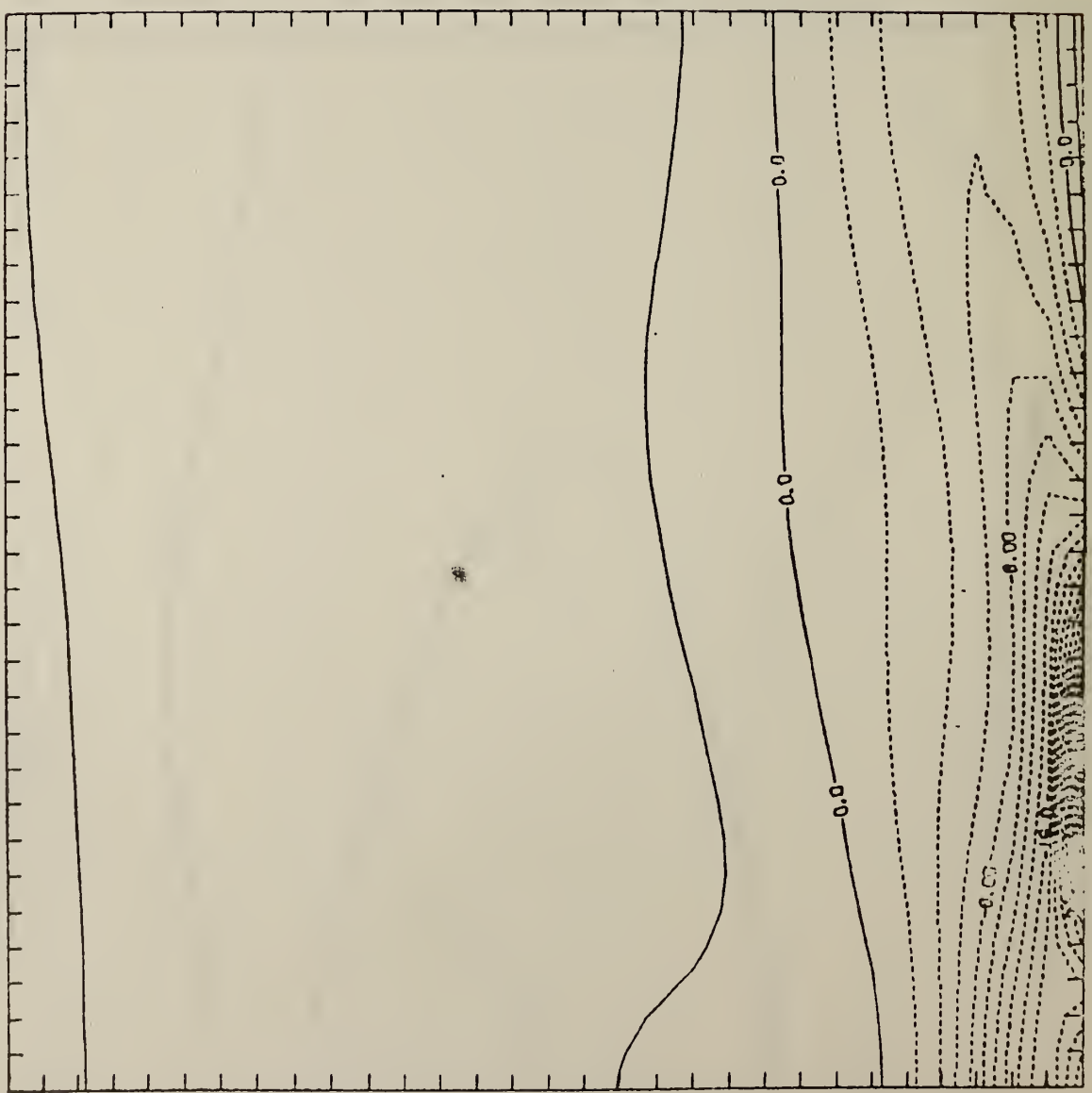

C.3. Heating in a Stratified, Two-Layer Fluid by a Noncentered Heat Source

In the final example all parameters are as described in the previous case except that the background density stratification changes abruptly at $y \tilde{=} 0.4$, the fluid being of uniform density below this location. Figure 24 shows plots of constant-perturbation-density at $t = 6.0$ in this calculation. This figure is shown only to demonstrate the qualitatively different behavior which occurs when the background density is composed of two layers, the upper one of variable density and the lower one of constant density (homogeneous). In the lower layer the profiles are qualitatively similar to what would be expected for heating in a homogeneous fluid. The structure in the upper layer is qualitatively quite different, showing what appears to be much detailed structure superimposed upon some mild undulations. The detailed structure should not be seriously considered because the magnitude of these variations is small. On the basis of previous studies, Reference 10, the discretization errors expected for the mesh $M = N = 31$ is of the order of a few percent. (It could be somewhat larger because the background density has a discontinuity in its gradient between the upper and lower layers.) The magnitude of the variations of the detailed structure is smaller than the expected discretization errors.

FIGURE 24

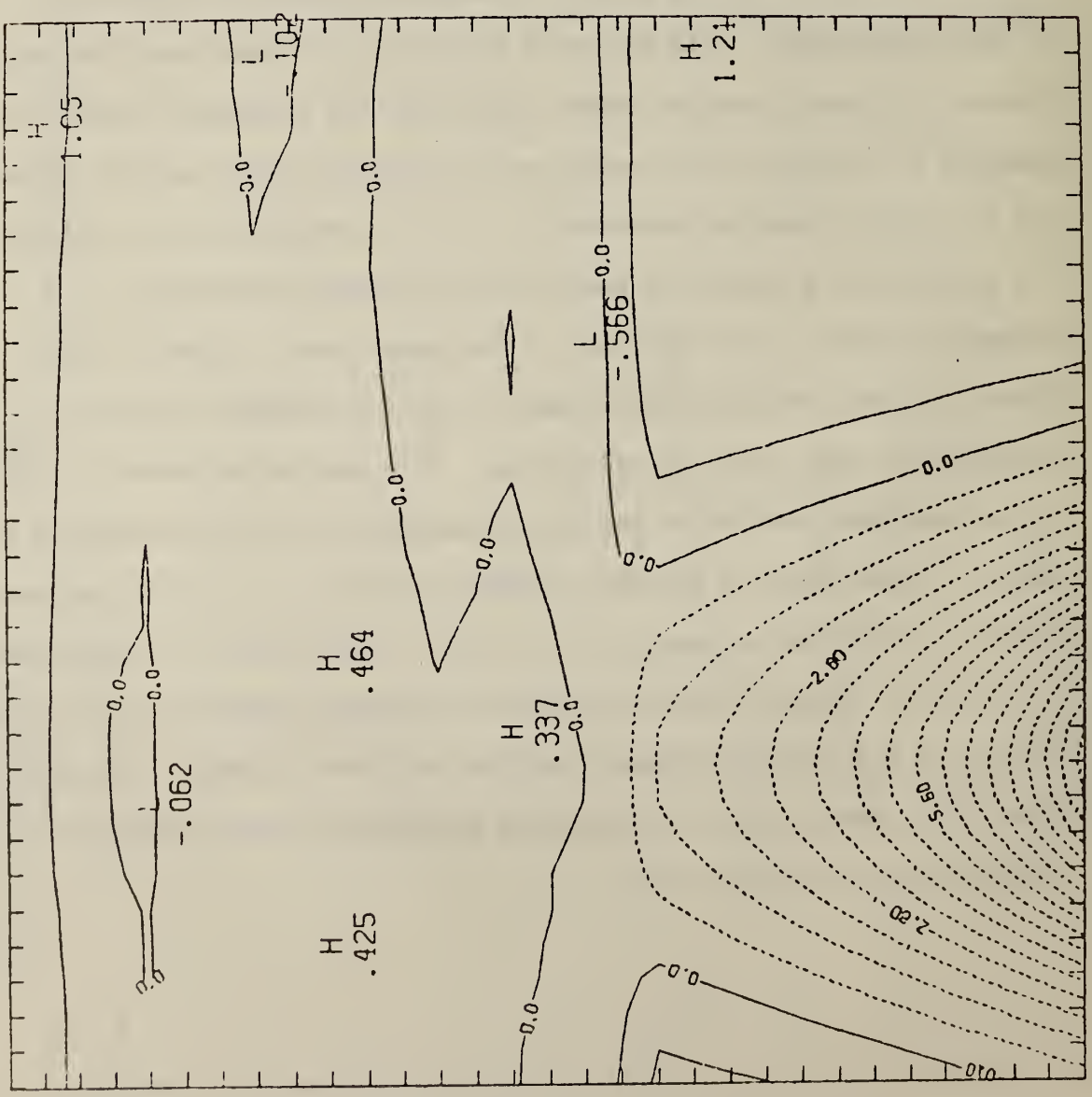
DENSITY CONTOUR MAP AT T = 6.00000+00
H 1.65
L -.102
H .464
H .425
H .337
L -.566
H 1.21
-.062
0.0
2.60
5.60
CONTOUR FROM -11.200 TO .70000 CONTOUR INTERVAL OF 70000 PTS3.3: -1.5075

VII. Summary

In an earlier paper[4] the equations of motion for thermally driven buoyant flows were derived. These approximate equations are applicable to nondissipative, highly nonadiabatic, buoyant flows of a perfect gas in which the heat is added slowly by a prescribed source. The equations were derived by assuming that the time scale associated with increase of the heat source is long compared with the transit time of an acoustic signal across the spatial extent of the source. Such an assumption is appropriate for buoyant flows produced by room fires. The resulting equations admit internal-wave motions while filtering out high-frequency acoustic waves. They are a generalization of the Boussinesq equations valid for nearly isobaric flows with large density and temperature differences. This combination of phenomena has not been extensively examined in studies of fluid flows.

In the present paper these nonlinear equations were recast in a form in which they could be integrated by finite difference techniques. In three dimensions the recast equations consist of three evolution equations, for density and the three components of velocity, along with a linear, nonseparable elliptic equation for the spatially variable portion of the pressure. (The mean pressure as a function of time is obtained by solving an ordinary differential equation). The formulation in which these fluid quantities are used as dependent variables is often refered to as a primitive variable or primitive equation formulation.

The equations were then made dimensionless, specialized to two dimensions and linearized. Finite difference approximations, second order accurate in both space and time, were made to the linearized equations. The dependent variables are density, the horizontal and vertical velocity components and pressure, and these variables are defined at various positions

within a grid cell (see Figure 1b).

The leapfrog procedure was used to determine the time evolution of the difference equations. To start the scheme, a first-order accurate scheme is used for the first time step. The computer time required for various size computations was reported.

At each time step, a system of linear algebraic equations, the finite difference approximation to the elliptic equation for the pressure, must be solved. The linear algebraic system of equations can be written in matrix form, in which case the coefficient matrix for the vector of unknown pressure values at grid points is large and sparse. It is important to utilize storage carefully and solve this algebraic system efficiently and accurately since the system is embedded in the larger fluid calculation and it must be solved repetitively. A hybrid method, combining the interactive algorithm called conjugate gradients with a fast direct method for solving Poisson's equation, was used to solve the algebraic system. (It was found typically that the solution of the algebraic equations arising on a 31 x 31 mesh could be determined to five significant figures after between two and five iterations of the conjugate gradients algorithm in between two to five seconds of CPU time on the N.B.S. UNIVAC 1108.)

Finally, results of some computations were presented using computer-generated plots. A discussion was given of the software required to generate these plots. A very brief discussion was presented of the analytical procedures required to obtain a solution to the differential equations describing heating of a homogeneous fluid. Computations of the

solution to the difference equations were found to confirm the conclusions of the analysis. Also these computations are found to yield flow fields which behave qualitatively the same as flow fields observed in a room fire. Examples of computations of the flow fields induced by heating in a stratified fluid were also presented and discussed.

References

1. Chandrasekhar, S., Hydrodynamic and Hydromagnetic Stability, Oxford University Press, 1961.

2. Swarzschild, M., Structure and Evolution of the Stars, Princeton University Press, Princeton, N.J., 1958.

3. Turner, J.S., Buoyancy Effects in Fluids, Cambridge University Press, Cambridge England, 1973.

4. Rehm, R.G. and Baum, H.R., The Equations of Motion for Thermally Driven, Buoyant Flows, Journal of Research of the National Bureau of Standards, Vol. 83, No. 3, May-June 1978, pp. 297-308.

5. Richtmyer, R.D. and Morton, K.W., Difference Methods for Initial-Value Problems, Wiley-Interscience, New York, 1967.

6. Harlow, F.H. and Amsden, A.A., Fluid Dynamics, ALASL Monograph, Los Alamos Scientific Laboratory Report LA4700, June 1971, Los Alamos, New Mexico.

7. Haltiner, G.J., Numerical Weather Prediction, John Wiley and Sons, Inc., New York, 1971.

8. Roache, P.J., Computational Fluid Dynamics, Hormosa Publishers, Albuquerque, N.M., 1976.

9. Kreiss, H. and Oliger, J., "Methods for the Approximate Solution of Time Dependent Problems", Global Atmospheric Research Programme (GARP) Publication Series No. 10, February 1973.

10. Baum, H.R. and Rehm, R.G., "Finite Difference Solutions for Internal Waves in Enclosures", National Bureau of Standards Report in preparation.

11. Schwarztrauber, P. and Sweet R., "Efficient FORTRAN Subprograms for the Solution of Elliptic Partial Differential Equations", NCAR-TN/IA-109, July, 1975.

12. Concus, P. and Golub, G., "Use of Fast Direct Methods for the Efficient Numerical Solution of Nonseperable Elliptic Equation", SIAM J. Numer. Anal., 10, 6, Dec. 1973.

13. Concus, P., Golub, G. and O'Leary, D.P., "A Generalized Conjugate Gradient Method for the Numerical Solution of Elliptic Partial Differential Equations", in Sparse Matrix Computations, J. Bunch & D. Rose, ed., pp. 309-332, Academic Press, New York, 1976.

14. Lewis, J. "The Numerical Solution of Pressure Equation by Hybrid Conjugate Gradients",

References

15. Cline, A.K., "Six subprograms for curve fitting using splines under tension", Comm. A.C.M. 17, 4 (April 1974) pp. 220-223.

16. Cline, A.K., "Scalar- and Planar-valued curve fitting using splines under tension", Comm. A.C.M. 17, 4 (April 1974) pp. 218-220.

17. Tektronix Plot 10 Advanced Graphing II User's Manual, Tektronix, Inc., September 1975.

18. Tektronix Plot 10 Terminal Control System User Manual, Tektronix, Inc., February 1977.

19. NCAR Graphics Software, edited by Tom Wright, NCAR Technical Note (preliminary edition), April 1977.

20. Meijer, J.E., "Hydrodynamic Models for the Treatment of Reactor Thermal Transients", Nuclear Science and Engineering, 10 (1961), pp. 269-277.

21. Porsching, T.A., "A Finite Difference Method for Thermally Expandable Fluid Transients", Nuclear Science and Engineering, 64, (1977) pp. 177-186; also Stewart, C.W. and George, T.L., "A Eulerian Computation Method for Fluid Flows with Large Density Gradients at all Speeds", Nuclear Science and Engineering, 64, (1977) pp. 237-243.

22. Dorr, F.W., "The Direct Solution of the Discrete Poisson Equation on a Rectangle", SIAM Review, 12, (April 1970), pp. 248-263.

NBS-114A (REV. 9-78)

U.S. DEPT. OF COMM. BIBLIOGRAPHIC DATA SHEET	1. PUBLICATION OR REPORT NO. NBSIR 79-1754	2. Gov't. Accession No.	3. Recipient's Accession No.

4. TITLE AND SUBTITLE

A Linearized Finite-Difference Computation of Fluid Heating in an Enclosure.

5. Publication Date May 1979

6. Performing Organization Code

7. AUTHOR(S) Ronald G. Rehm, Howard R. Baum, John Lewis, and Martin R. Cordes.

8. Performing Organ. Report No.

9. PERFORMING ORGANIZATION NAME AND ADDRESS

NATIONAL BUREAU OF STANDARDS
DEPARTMENT OF COMMERCE
WASHINGTON, DC 20234

10. Project/Task/Work Unit No.

11. Contract/Grant No.

12. SPONSORING ORGANIZATION NAME AND COMPLETE ADDRESS *(Street, City, State, ZIP)*

SAME AS ITEM 9

13. Type of Report & Period Covered Interim

14. Sponsoring Agency Code

15. SUPPLEMENTARY NOTES

☐ Document describes a computer program; SF-185, FIPS Software Summary, is attached.

16. ABSTRACT *(A 200-word or less factual summary of most significant information. If document includes a significant bibliography or literature survey, mention it here.)* In an earlier paper, approximate equations of motion were derived which are applicable to nondissipative, very nonadiabatic, buoyant flows of a perfect gas. In the present paper, these approximate equations are recast in a form in which they can be integrated by finite difference techniques. The nonlinear equations are made dimensionless, specialized to two dimensions and linearized. Finite difference approximations, using central differences in space and leapfrog in time, are made to the linearized equations. To start the computation, a first-order scheme is used for the initial time step. The dependent variables are density, the horizontal and vertical velocity components and pressure, and these variables are defined at various positions within a grid cell. The computer time required for various size computations and the accuracies obtained are reported.

At each time step, a large sparse system of linear algebraic equations, the finite difference approximation to the elliptic equation for the pressure, must be solved. A hybrid method, combining the interactive algorithm called conjugate gradients with a fast direct method for solving Poisson's equation, is used to solve the algebraic system efficiently and accurately. Examples of computations of the flow fields induced by heating are presented and discussed.

17. KEY WORDS *(six to twelve entries; alphabetical order; capitalize only the first letter of the first key word unless a proper name; separated by semicolons)* Buoyant convection; finite - difference computations; fire in an enclosure; heat addition; hyperbolic, elliptic equations; initial, boundary - value problem; linearized equations; partial differential equations.

18. AVAILABILITY ☒ Unlimited

☐ For Official Distribution. Do Not Release to NTIS

☐ Order From Sup. of Doc., U.S. Government Printing Office, Washington, DC 20402, SD Stock No. SN003-003-

☒ Order From National Technical Information Service (NTIS), Springfield, VA. 22161

19. SECURITY CLASS (THIS REPORT)	21. NO. OF PRINTED PAGES
UNCLASSIFIED	76
20. SECURITY CLASS (THIS PAGE)	**22. Price**
UNCLASSIFIED	$6.00

USCOMM-DC